Perceptive Mobile Networks for Standalone and Cooperative UAV Surveillance

Yue Zhang, Hangguan Shan, *Senior Member, IEEE,* Hongbin Chen, Lin Cai, *Fellow, IEEE,* Zhiguo Shi, *Senior Member, IEEE,* Tony Q. S. Quek, *Fellow, IEEE*, and Li Sheng

***Abstract*—The next-generation wireless network is perceived to integrate with sensing capability and evolve into the perceptive mobile network (PMN), enabling massive sensing-intensive applications. However, the sensing function will affect the communication performance in cellular networks. To study the sensing and communication performance of PMNs and their interactions, this paper investigates a millimeter-wave PMN with dual-functional base stations (BSs) for simultaneous detection of unauthorized unmanned aerial vehicles (UAVs) and user communication via the unified transmit signal and beamforming. We develop a system-level theoretical framework to investigate the sensing and communication performance of PMNs based on stochastic geometry, which captures the mutual interference and resource contention between the two functions and builds a foundation for the optimization of network configurations. In addition, by leveraging the collaboration of multiple BSs in PMNs, we propose a cooperative sensing strategy combining the monostatic and bistatic sensing processes to enhance the reliability of UAV surveillance. Simulation results verify the effectiveness of the proposed theoretical framework and demonstrate the benefits of cooperative sensing in UAV detection and communication performance, as compared with the standalone sensing by individual BSs.**

***Index Terms*—Perceptive mobile network, integrated sensing and communication, UAV surveillance, cooperative sensing.**

I. Introduction

THE wireless network is undergoing a paradigm shift from the communication-only network to the perceptive mobile network (PMN) with intrinsic sensing capability [1]. With the support of the integrated sensing and communication (ISAC) technology, the PMN is expected to perform dual functions of sensing and communication on the unified hardware platforms via sharing the same millimeter-wave (mmWave) frequency band [2, 3]. PMNs can achieve networked sensing with minor modifications on current cellular infrastructures, thus enabling a variety of sensing-intensive applications including the unmanned aerial vehicle (UAV) surveillance [4, 5]. With high mobility and low cost, UAVs have been pervasively used in civil and military fields, such as product delivery, assisted networking, and reconnaissance [6, 7]. However, in the absence of comprehensive surveillance, the unauthorized UAVs may pose severe security threats, such as illegal data collection, aerial collision, and even terrorist attack [8]. Leveraging the PMN for UAV surveillance can avoid the prohibitively high costs of deploying dedicated cameras and acoustic sensors over expansive areas, and also overcome their vulnerability to weather and light conditions [7].

Exploiting PMNs for UAV surveillance brings both challenges and opportunities. On one hand, the joint communication and UAV detection conducted by a base station (BS) introduces dual-functional interference and resource contention [3]. In addition, the simultaneous UAV sensing performed by the large-scale BSs in PMNs leads to mutual interference and network clutter. How to configure the large number of BSs in PMNs to realize both sensing and communication functions and how to reveal the interplay between the two functions have not been thoroughly investigated yet [2]. On the other hand, the distributed yet interconnected BSs in PMNs offer promising opportunities for cooperative sensing [9, 10]. This enables the collaborative utilization of the multiple perspectives from different BSs for sensing a UAV, and thus acquires spatial diversity gain and wide angular observations and improves the reliability of UAV detection [11]. Researches on the cooperative sensing in PMNs as well as the corresponding dual-functional performance are still in the infancy. To fill the gap, this paper considers the following problems:

- How to build a general theoretical framework to analyze the communication and sensing performance of PMNs?
- How to design the cooperative sensing strategy in PMNs to enhance UAV detection performance compared with standalone sensing?
- How to fine tune network configurations to optimize the dual-functional performance of PMNs?

Manuscript received 5 October, 2023; revised 13 April and 31 August, 2024; accepted 17 October, 2024. This work was supported in part by the National Natural Science Foundation of China (NSFC) under Grants U21A20456 and U21B2029, in part by the Zhejiang Provincial Natural Science Foundation of China under Grant LR23F010006, in part by the Science and Technology Development Fund (SKLIOTSC(UM)-2024-2026), in part by the State Key Laboratory of Internet of Things for Smart City (University of Macau) (Ref. No.: SKL-IoTSC(UM)-2024-2026/ORP/GA01/2023), and in part by the National Research Foundation, Singapore and Infocomm Media Development Authority under its Future Communications Research & Development Programme. The associate editor coordinating the review of this article and approving it for publication was Kamel Tourki. *(Corresponding authors: Hangguan Shan; Tony. Q. S. Quek)*

Yue Zhang, Hangguan Shan, and Zhiguo Shi are with the College of Information Science and Electronic Engineering, Zhejiang University, Hangzhou 310027, China (e-mail: zhangyuezy@zju.edu.cn; hshan@zju.edu.cn; shizg@zju.edu.cn).

Hongbin Chen is with the School of Information and Communication, Guilin University of Electronic Technology, Guilin 541004, China (e-mail: chbscut@guet.edu.cn).

Lin Cai is with the Department of Electrical and Computer Engineering, University of Victoria, Victoria, BC V8P 5C2, Canada (e-mail: cai@ece.uvic.ca).

Tony Q. S. Quek is with the Singapore University of Technology and Design, Singapore 487372, and also with the Yonsei Frontier Lab, Yonsei University, Seoul 03722, South Korea (e-mail: tonyquek@sutd.edu.sg).

Li Sheng is with the Huaxin Consulting Design & Research Institute Co., Ltd., Hangzhou 310056, China (e-mail: shengli.hx@chinaccs.cn).

In this paper, first, we establish an analytical framework for quantifying both sensing and communication performance of the mmWave UAV surveillance-oriented PMN, where the BSs in the PMN are responsible for providing downlink communication service to ground user equipments (GUEs) and detecting the unauthorized UAVs around them at the same time. Two ways for BSs to conduct UAV detection are considered, namely, the standalone sensing by individual BSs, and the cooperative sensing by multiple BSs leveraging a hybrid of monostatic sensing and bistatic sensing, respectively. Specifically, the theoretical expressions for rate coverage probability (RCP), successful detection probability (SDP), and sensing outage probability (SOP) are derived based on stochastic geometry. By optimizing the network configurations in terms of the allocation of power and radio frequency (RF) chain resources, BS density, and sensing coverage of BSs, we investigate the enhancement and tradeoff of sensing and communication performance for the PMN. The main contributions of this paper are summarized as follows:

- From the dual-functional perspective, we explore how the PMN can achieve reliable UAV surveillance and user communication simultaneously by investigating the ISAC signal, beamforming, and sensing coverage, and propose a cooperative sensing strategy for reliable UAV detection.
- Based on stochastic geometry, we establish a system-level theoretical framework for analyzing the sensing and communication performance of PMNs in standalone and cooperative sensing cases, capturing the mutual interference and resource contention between the two functions.
- Based on the proposed theoretical framework, we investigate the different impacts of key network parameters on sensing and communication performance, and shed some light on dual-functional resource allocation and network configuration of PMNs.

The rest of this paper is organized as follows. In Section II, we overview the related work. The system model of the mmWave UAV surveillance-oriented PMN is described in Section III. In Section IV, we elaborate on the standalone and cooperative sensing in the PMN. In Section V, we establish the analytical framework for sensing and communication performance of PMNs, and the performance optimization is studied in Section VI. Simulation results are given in Section VII. Finally, the paper is concluded in Section VIII.

Notations: The lowercase and uppercase bold letters are used for vectors and matrices, respectively. $(\cdot)^{\mathrm{T}}$ and $(\cdot)^{\mathrm{H}}$ stand for the transpose and conjugate transpose, respectively. $\mathbf{I}_N$ denotes the identity matrix of dimension $N \times N$. $\mathbb{N}$ denotes the set of natural numbers. $\mathbb{C}^{x\times y}$ denotes the space of $x \times y$ complex matrices. $|z|$ denotes the absolute value of z. $\|\mathbf{x}\|$ denotes the Euclidean norm of a complex vector $\mathbf{x}$. $\sim$ stands for "distributed as". $\mathrm{Gamma}(a, b)$ denotes the Gamma distribution with a and b being the shape and rate parameters, respectively. $\Gamma(\cdot)$ is the Gamma function. $\mathbf{1}(A)$ is the indicator function, equal to 1 when event A occurs and 0 otherwise.

II. Related Work

For the dual-functional PMN, a number of existing studies have investigated the dual-functional interference, resource contention, and performance tradeoff between sensing and communication. Some early studies focus on the mutual interference mitigation via time-division [1] or opportunistic spectrum access [12] for sensing and communication, which leads to low degree of integration of the two functions and causes low resource utilization and extra control overhead. The authors of [3, 13] design the ISAC waveform and beamforming and optimize the dual-functional power allocation to enhance the accuracy of parameter estimation, taking into account the mutual interference between sensing and communication while ignoring the clutter in target sensing. In the presence of clutter patches in background environments, a beamforming management method for the mutual interference suppression between sensing and communication is proposed in [14] for PMNs, with one BS acting as the signal transmitter and one target monitoring terminal (TMT) acting as the echo receiver. Moreover, a unified framework for the performance of target detection, localization, and tracking is proposed and the allocation of power and bandwidth resources between sensing and communication is optimized in [5], where the clutter suffered by a BS is modeled as a Gaussian random variable same as the noise.

In view of the potential spatial diversity gain of cooperative sensing, several studies investigate the feasible cooperative sensing structures for PMNs, as well as the fusion policy for the sensing results from multiple BSs. A distributed PMN architecture for cooperative sensing is proposed in [11], where several TMTs are added only as sensing receivers and the BS is dedicated as the sensing transmitter. Another cooperative architecture proposed in [9] integrates sensing into the cloud radio access network (C-RAN), where part of the remote radio units are used as sensing receivers and the others are transmitters. Flexible cooperative sensing structures are introduced in [10] by combining the monostatic, bistatic, and multi-static sensing processes. With cooperation, the signals sent by multiple transmitters for sensing the target experience different transmission links to the receivers, and the spatial diversity gain can be acquired by jointly processing the echoes at multiple receivers. The fusion rules and cooperative BS selection policy in PMNs are studied in [15], where the binary detection decisions from multiple BSs are fused at the central node. The multi-radar cooperative detection system is introduced in [16] to obtain better detection capability by fusing the original echoes received at multiple radars through broadband networks.

Different from the existing work studying a limited number of BSs, we focus on the new challenges of integrating sensing function into conventional cellular networks with the large-scale and randomly distributed BSs, and provide system-level analysis on sensing and communication performance. We aim to shed some light on network configurations for clutter suppression, mutual interference reduction, and performance optimization of the dual-functional PMN. Furthermore, we investigate the cooperative sensing strategy for PMNs with the collaboration of interconnected BSs, and reveal the benefits of cooperative sensing on both UAV detection and sensing coverage performance.

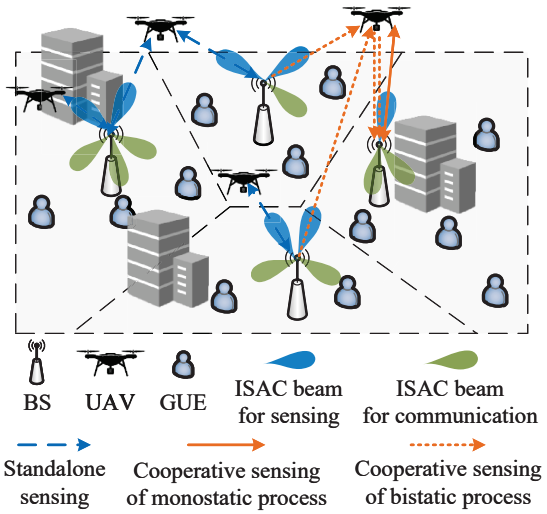

Fig. 1: Illustration of the PMN supporting UAV surveillance.

III. System Model

In this section, the system model of the mmWave PMN for UAV surveillance is presented. Specifically, we introduce the stochastic geometry model, antenna model, association policy, ISAC signal and beamforming model, and channel model.

A. Stochastic Geometry Model

As shown in Fig. 1, we consider a mmWave cellular network where BSs are deployed to simultaneously serve GUEs and detect unauthorized UAVs that neither communicate nor provide information to BSs. The locations of BSs, UAVs, and GUEs are modeled by two-dimensional (2D) homogeneous Poisson point processes (HPPPs) Φ_{B}, Φ_{U}, and Φ_{G} with densities λ_{b}, λ_{u}, and λ_{g} at constant heights H_{B}, H_{U}, and 0, respectively.[1] In this paper, we focus on downlink transmissions which also incorporate the sensing function, and the uplink communication can work under time or frequency duplex division to avoid the interference with downlink signals and echoes, given sufficient time or frequency guard intervals [2, 18]. In addition, we assume that the locations of GUEs and UAVs are unchanged within the short time of one signal transmission and reception process. Our analysis is based on a randomly chosen BS from Φ_{B}, denoted as the typical BS by $\mathbf{x}$, whose location is set as the origin of the coordinate system.

B. Antenna Model

Due to the severe penetration loss in mmWave band, we consider that BSs are equipped with uniform planar arrays (UPAs) with N_{t} and N_{r} antennas for signal transmission and reception, respectively. Assume that the transmit and receive UPAs at BSs are well-separated and sufficiently isolated to avoid the interference between echoes and transmit signals [9]. In addition, GUEs are equipped with omni-directional antennas to ensure the signal reception from BSs [19]. Assume that the UPAs at the typical BS are placed in the x-z plane. For analytical tractability, we adopt the array response vector of UPA based on virtual angles as [20]

$$\mathbf{a}_w(\phi,\theta)=\tfrac{1}{\sqrt{N_w}}\left[1,\ldots,e^{j(m\phi+n\theta)},\ldots,e^{j[(N_{w,\mathrm{az}}-1)\phi+(N_{w,\mathrm{el}}-1)\theta]}\right]^{\mathrm{T}}. \tag{1}$$

Here, $\phi = \frac{2\pi}{\lambda}d\cos\psi\sin\gamma, \phi \in [-\pi,\pi]$ and $\theta = \frac{2\pi}{\lambda}d\cos\gamma, \theta\in[-\pi,\pi]$ are the virtual azimuth angle and virtual elevation angle, respectively. $\psi\in[0,2\pi]$ and $\gamma\in[0,\pi]$ are the physical azimuth and elevation angles of signals relative to UPAs, representing the angles between the x-axis and the projection of signals on the x-y plane, and angles between the z-axis and signals, respectively. Owing to the nonlinearity in the angular domain of the array response vector with physical angles, the representation with virtual angles is adopted. $N_w = N_{w,\mathrm{az}}N_{w,\mathrm{el}}$, with $w\in\{\mathrm{t},\mathrm{r}\}$ denoting "transmit" or "receive". $N_{w,\mathrm{az}}$ and $N_{w,\mathrm{el}}$ are the numbers of antennas in the azimuth and elevation directions, respectively. λ is the signal wavelength, and d is the spacing between adjacent antenna elements and set to $\lambda/2$ [21].

Due to the limited angular resolution of UPAs with finite antenna aperture, the signals from pretty close angles are unresolvable. Thus, the virtual azimuth and elevation angles within $[\frac{2\pi(m-1)}{N_{w,\mathrm{az}}},\frac{2\pi m}{N_{w,\mathrm{az}}})$ and $[\frac{2\pi(n-1)}{N_{w,\mathrm{el}}},\frac{2\pi n}{N_{w,\mathrm{el}}})$ are quantized to take values of $\phi_m=\frac{2\pi m}{N_{w,\mathrm{az}}}$, $m=1,2,\ldots,N_{w,\mathrm{az}}$ and $\theta_n=\frac{2\pi n}{N_{w,\mathrm{el}}}$, $n=1,2,\ldots,N_{w,\mathrm{el}}$, respectively [20]. The antenna gain of UPAs is given by $\left|\mathbf{a}_w^{\mathrm{H}}(\phi_{m_1},\theta_{n_1})\mathbf{a}_w(\phi_{m_2},\theta_{n_2})\right|^2 = G_w^2\mathbf{1}[(m_1=m_2)\&(n_1=n_2)]+g_w^2\mathbf{1}[(m_1\neq m_2)\,|\,(n_1\neq n_2)]$, $w\in\{\mathrm{t},\mathrm{r}\}$. Based on (1), the main lobe antenna gain G_w^2 equals 1, and the side lobe antenna gain g_w^2 equals 0 owing to the orthogonality among the array response vectors with quantized virtual angles. But, to avoid the underestimation of interference, g_w^2 is set to be nonzero similar to [20].

C. Association Policy

1) GUE Association

The GUEs associate with their nearest BSs for communication. Considering the constraints on antenna and RF chain resources, we assume that a BS can communicate with at most $K_{\max}$ GUEs simultaneously in the same frequency band. If the number of GUEs in the coverage area of a BS exceeds the maximal value, then $K_{\max}$ GUEs are randomly selected to associate with the BS. Based on the property of HPPP distributions, the probability mass function (PMF) of the total number of GUEs in the coverage area of a BS, K_{G}, is given as [22]

$$\mathbb{P}(K_{\mathrm{G}}=i)=\frac{h^h\Gamma(i+h)(\frac{\lambda_{\mathrm{g}}}{\lambda_{\mathrm{b}}})^i}{i!\Gamma(h)(h+\frac{\lambda_{\mathrm{g}}}{\lambda_{\mathrm{b}}})^{i+h}}, i\in\mathbb{N}, \tag{2}$$

where h is a dimension-related index and takes the value of $(3\varpi+1)/2$, with ϖ being the dimension of the HPPP distribution of BSs. Because here we consider the 2D distributed BSs, ϖ equals 2 and thus h equals 3.5 [23]. As given above, the PMF of the number of GUEs within the coverage area of a BS is dependent on the densities of BSs and GUEs. Consider that there are K_0 GUEs in the coverage area of the typical BS, then the number of associated GUEs of the typical BS,

[1]The theoretical framework in this paper is also applicable for the network performance of three-dimensional (3D) distributed UAVs with uniformly distributed heights [17], which is verified in simulations in Section VII.

K, equals $\min\{K_0, K_{\max}\}$. The probability density function (PDF) of the horizontal distance between the typical BS and its $k^{\text{th}}, k \in \{1, 2, \ldots, K\}$ associated GUE (denoted by the typical GUE), v_0, can be given by $f_{\text{G}}(v_0) = 2\pi\lambda_{\text{b}} v_0 \exp\left(-\pi\lambda_{\text{b}} v_0^2\right)$ [22].

Given the HPPP distribution of GUEs on the ground, the joint PDF of the virtual azimuth and elevation angles of an arbitrary GUE, other than the K associated GUEs, relative to the typical BS is derived in Appendix A as

$$f_{\text{C}}^{(\text{ar})}(\phi, \theta) = \frac{2\pi H_{\text{B}}^2}{D^2 |\theta|^3 \sqrt{\pi^2 - \phi^2 - \theta^2}}, \tag{3}$$

where D is the radius of the network, and for HPPP models, $D \to \infty$. $\phi \in [-\pi, \pi]$ and $\theta \in [-\pi, \frac{-\pi H_{\text{B}}}{\sqrt{D^2 + H_{\text{B}}^2}}]$. As for the virtual azimuth and elevation angles of the typical GUE relative to the typical BS, their joint PDF can be derived similar to (3) as

$$f_{\text{C}}^{(\text{ty})}(\phi, \theta) = 2\lambda_{\text{b}} \exp\left(-\pi\lambda_{\text{b}} H_{\text{B}}^2 \frac{\pi^2 - \theta^2}{\theta^2}\right) \frac{\pi^2 H_{\text{B}}^2}{|\theta|^3 \sqrt{\pi^2 - \phi^2 - \theta^2}}. \tag{4}$$

2) Target UAV

In addition to communicating with GUEs, BSs are also responsible for detecting the unauthorized UAVs around them. In the initial stage of UAV detection, all BSs sense the environment in an omni-directional manner to acquire rough information of UAV locations for beam alignment. In the next detection stage, based on the initial observations, BSs transmit directional beams to detect the UAVs that are within a horizontal distance R_{S} (termed as the sensing distance) for further observation [3]. We consider that a BS can sense at most $Q_{\max}$ UAVs at the same time via the same transmit signal. If the total number of UAVs in the sensing area of a BS Q_{U} exceeds $Q_{\max}$, the BS randomly selects $Q_{\max}$ UAVs as target UAVs for sensing. The PMF of Q_{U} is obtained by

$$\mathbb{P}(Q_{\text{U}} = j) = \frac{(\lambda_{\text{u}} \pi R_{\text{S}}^2)^j}{j!} \exp\left(-\lambda_{\text{u}} \pi R_{\text{S}}^2\right), j \in \mathbb{N}, \tag{5}$$

which holds owing to the Poisson property of HPPP. Given Q_0 UAVs within the sensing area of the typical BS, the number of the target UAVs of the typical BS, Q, equals $\min\{Q_0, Q_{\max}\}$. Then, the PDF of the horizontal distance between the typical BS and its q^{th} ($q \in \{1, 2, \ldots, Q\}$) target UAV (denoted by the typical UAV), r_0, can be given by $f_{\text{U}}(r_0) = \frac{2r_0}{R_{\text{S}}^2}$.

Consider that UAVs hover at a higher altitude than BSs, the joint PDF of the virtual azimuth and elevation angles of a UAV relative to the typical BS can be derived as

$$f_{\text{S}}^{\mathcal{M}}(\phi, \theta) = \frac{2\pi \Delta H^2}{D^{(\mathcal{M})^2} |\theta|^3 \sqrt{\pi^2 - \phi^2 - \theta^2}}, \tag{6}$$

where $\phi \in [-\pi, \pi]$, $\theta \in [\frac{\pi \Delta H}{\sqrt{D^{(\mathcal{M})^2} + \Delta H^2}}, \pi]$, $\mathcal{M} \in \{\text{ty}, \text{ar}\}$ denotes "typical" or "arbitrary", representing the typical UAV or an arbitrary UAV other than the Q target UAVs, $D^{(\text{ty})} = R_{\text{S}}$, $D^{(\text{ar})} = D$, and $\Delta H = H_{\text{U}} - H_{\text{B}}$. Equation (6) can be proved with the similar approach in Appendix A.

Based on the PDFs analyzed above and the quantized virtual angles given in Section III-B, the PMF of the quantized virtual azimuth and elevation angles of GUEs and UAVs relative to the typical BS, $\phi_m, m = 1, 2, \ldots, N_{w,\text{az}}$ and $\theta_n, n = 1, 2, \ldots, N_{w,\text{el}}$, can be further obtained by

$$p_{\mathcal{O},w}^{(\mathcal{M})}(\phi_m, \theta_n) = \int_{\phi_m - \frac{\pi}{N_{w,\text{az}}}}^{\phi_m + \frac{\pi}{N_{w,\text{az}}}} \int_{\theta_n - \frac{\pi}{N_{w,\text{el}}}}^{\theta_n + \frac{\pi}{N_{w,\text{el}}}} f_{\mathcal{O}}^{(\mathcal{M})}(\phi, \theta) \text{d}\theta \text{d}\phi, \tag{7}$$

where $\mathcal{O} \in \{\text{C}, \text{S}\}$ represents "communication" or "sensing".

D. ISAC Signal and Beamforming Model

For the PMN, the unified ISAC signal $\mathbf{X}$ is transmitted by the typical BS to its K associated GUEs and Q target UAVs, which is expressed as [13]

$$\mathbf{X} = \mathbf{W}\mathbf{S}, \ \mathbf{X} \in \mathbb{C}^{N_{\text{t}} \times T}, \tag{8}$$

where T is the length of transmit data symbols, $\mathbf{W} \in \mathbb{C}^{N_{\text{t}} \times (K+Q)}$ is the transmit beamforming matrix to be designed in further detail below, and $\mathbf{S} \in \mathbb{C}^{(K+Q) \times T}$ is the data symbol matrix given as $\mathbf{S} = [\mathbf{s}_{\text{C},1}, \ldots, \mathbf{s}_{\text{C},k}, \ldots, \mathbf{s}_{\text{S},q}, \ldots \mathbf{s}_{\text{S},Q}]^{\text{T}}$.[2] Here, $\mathbf{s}_{\text{C},k} \in \mathbb{C}^{T \times 1}$ represents the downlink communication symbols for the typical GUE k, and $\mathbf{s}_{\text{S},q} \in \mathbb{C}^{T \times 1}$ represents the dedicated sensing symbols for the typical UAV q, generally being predefined symbols of constant modulus and containing no useful communication data [14]. $\mathbf{s}_{\text{S},q}$ is specifically added to provide extra degrees of freedom for multiple target sensing and enhance the determinism of the ISAC signal, which contributes to guaranteeing unbiased estimation and balancing the deterministic-random tradeoff between sensing and communication symbols [14, 25]. Communication-centric, radar-centric, or co-design waveforms can be adopted herein for $\mathbf{s}_{\text{C},k}$ and $\mathbf{s}_{\text{S},q}$ [13, 18, 26]. In addition, the transmit data symbols for different GUEs and UAVs are assumed to be uncorrelated with each other [27], i.e., $\mathbb{E}[\mathbf{S}\mathbf{S}^H] = T\mathbf{I}_{K+Q}$.

To elaborate on the dual-functional contention for power resources, the total transmit power P_{t} is allocated between communication and sensing functions by each BS with power allocation coefficient ρ. To study the average performance of GUEs and UAVs, the transmit power for communication $P_{\text{t,C}} = \rho P_{\text{t}}$ and that for sensing $P_{\text{t,S}} = (1 - \rho) P_{\text{t}}$ are equally allocated by each BS to its associated GUEs and target UAVs, respectively, according to its own traffic load. Under the constraint of hardware cost, the hybrid analog-digital (HAD) transmit beamforming is adopted with a limited number of RF chains [28]. To achieve simultaneous user communication and UAV detection, the HAD transmit beamforming matrix $\mathbf{W}$ in (8) is designed as

$$\mathbf{W} = \mathbf{F}_{\text{RF}} \mathbf{F}_{\text{BB}} = [\mathbf{w}_{\text{C},\mathbf{x},1}, \ldots, \mathbf{w}_{\text{C},\mathbf{x},k}, \ldots, \mathbf{w}_{\text{S},\mathbf{x},q}, \ldots, \mathbf{w}_{\text{S},\mathbf{x},Q}], \tag{9}$$

where $\mathbf{F}_{\text{RF}} = [\mathbf{a}_{\text{t}}(\phi_{\text{C},\mathbf{x},1}, \theta_{\text{C},\mathbf{x},1}), \ldots, \mathbf{a}_{\text{t}}(\phi_{\text{C},\mathbf{x},k}, \theta_{\text{C},\mathbf{x},k}), \ldots, \mathbf{a}_{\text{t}}(\phi_{\text{S},\mathbf{x},q}, \theta_{\text{S},\mathbf{x},q}), \ldots, \mathbf{a}_{\text{t}}(\phi_{\text{S},\mathbf{x},Q}, \theta_{\text{S},\mathbf{x},Q})] \in \mathbb{C}^{N_{\text{t}} \times N_{\text{RF}}}$ and $\mathbf{F}_{\text{BB}} = \text{diag}(\sqrt{P_{\text{t,C}}/K}, \ldots, \sqrt{P_{\text{t,C}}/K}, \ldots, \sqrt{P_{\text{t,S}}/Q}, \ldots, \sqrt{P_{\text{t,S}}/Q}) \in \mathbb{C}^{N_{\text{RF}} \times (K+Q)}$ are the RF beamforming matrix and baseband beamforming matrix of the typical BS $\mathbf{x}$, respectively; $\mathbf{w}_{\text{C},\mathbf{x},k} = \sqrt{P_{\text{t,C}}/K} \mathbf{a}_{\text{t}}(\phi_{\text{C},\mathbf{x},k}, \theta_{\text{C},\mathbf{x},k})$ and

[2]Note that the phase noise to mmWave ISAC signals, caused by the non-ideal hardware in practical systems, is assumed to be pre-eliminated via advanced estimation and compensation methods [24].

$\mathbf{w}_{\mathrm{S},\mathbf{x},q} = \sqrt{P_{\mathrm{t,S}}/Q}\mathbf{a}_{\mathrm{t}}(\phi_{\mathrm{S},\mathbf{x},q}, \theta_{\mathrm{S},\mathbf{x},q})$ are the transmit beamforming vectors for the typical GUE and the typical UAV, respectively;[3] $\phi_{\mathrm{C},\mathbf{x},k}$, $\theta_{\mathrm{C},\mathbf{x},k}$, $\phi_{\mathrm{S},\mathbf{x},q}$, and $\theta_{\mathrm{S},\mathbf{x},q}$ are the quantized virtual azimuth and elevation angles of the typical GUE and the typical UAV relative to $\mathbf{x}$, respectively, and taking values of $\phi_m, m = 1, 2, \ldots, N_{w,\mathrm{az}}$ and $\theta_n, n = 1, 2, \ldots, N_{w,\mathrm{el}}$ with probabilities shown in (7); and $N_{\mathrm{RF}} = K + Q$ is the number of RF chains with the maximum value of $N_{\mathrm{RF,max}}$, which limits the maximum capability of a BS for serving at most $K_{\max} = \eta N_{\mathrm{RF,max}}$ GUEs and for sensing at most $Q_{\max} = (1-\eta)N_{\mathrm{RF,max}}$ UAVs simultaneously, with η being the RF chain allocation coefficient.

E. Channel Model

In this paper, the vulnerability of mmWave signals to obstructions is taken into account. Whether the link between the typical BS and the typical GUE is line-of-sight (LoS) or non-line-of-sight (NLoS) transmission can be measured by a distance-dependent probability model [30]. The probability that the transmission link has an LoS path is

$$\mathbb{P}_{\mathrm{L}}(v_0) = \frac{1}{1 + a\exp\left[-b(\frac{180}{\pi}\tan^{-1}\frac{H_{\mathrm{B}}}{v_0} - a)\right]}, \tag{10}$$

where a and b are environment-related constants, and v_0 is the horizontal distance between the typical BS and the typical GUE. The NLoS probability is given as $\mathbb{P}_{\mathrm{N}}(v_0) = 1 - \mathbb{P}_{\mathrm{L}}(v_0)$.

The mmWave channels are expected to be sparse with the majority of energy being captured by several arrival and departure angles. Thus, the virtual channel approximation representation is adopted to characterize the mmWave channels in the angular domain based on the predefined quantized virtual angles [31]. Specifically, the downlink transmission from the typical BS $\mathbf{x}$ to the typical GUE k can be modeled by the communication channel vector $\mathbf{h}_{\mathbf{x},k}$ only containing the paths within the quantized virtual angle of the typical GUE as

$$\mathbf{h}_{\mathbf{x},k} = \sqrt{N_{\mathrm{t}}L_{\mathrm{C},\mathbf{x},k,e}}\beta_{\mathrm{C},\mathbf{x},k,e}\mathbf{a}_{\mathrm{t}}(\phi_{\mathrm{C},\mathbf{x},k}, \theta_{\mathrm{C},\mathbf{x},k}), \tag{11}$$

where $\beta_{\mathrm{C},\mathbf{x},k,e}$ denotes the Nakagami fading of the link between the typical BS and the typical GUE, with $\beta^2_{\mathrm{C},\mathbf{x},k,e}$ following Gamma distribution $\mathrm{Gamma}(m_e, m_e)$ and $m_e, e \in \{\mathrm{L}, \mathrm{N}\}$ being the Nakagami parameter of LoS or NLoS links; N_{t} here is for normalization; $L_{\mathrm{C},\mathbf{x},k,e} = \zeta(v_0^2 + H_{\mathrm{B}}^2)^{-\frac{\alpha_e}{2}}$ is the path loss of the link between the typical BS and the typical GUE, with α_e being the path loss exponent, $\zeta = (\frac{3\times10^8}{4\pi f_c})^2$ being the path loss intercept, and f_c denoting the carrier frequency. In this paper, similar to [22, 32], perfect channel estimation via reference signals is assumed.

Overall, the received signal at the typical GUE from the typical BS, $\mathbf{y}_{\mathrm{C},\mathbf{x},k}$, can be given as

$$\mathbf{y}_{\mathrm{C},\mathbf{x},k} = \mathbf{h}^{\mathrm{H}}_{\mathbf{x},k}\mathbf{X} + \mathbf{z}_{\mathrm{C},\mathbf{x},k}, \tag{12}$$

where $\mathbf{z}_{\mathrm{C},\mathbf{x},k} \in \mathbb{C}^{1\times T}$ is the additive white Gaussian noise (AWGN) vector of communication link, and each entry of $\mathbf{z}_{\mathrm{C},\mathbf{x},k}$ follows the circularly symmetric complex Gaussian (CSCG) distribution of variance $\sigma_{\mathrm{C}}B$, with σ_{C} denoting the noise power spectral density of communication links and B representing the signal bandwidth.

As for sensing processes, the UAVs are regarded as point-like targets. Considering that UAVs and BSs are deployed at certain heights, it is very likely to have an LoS path between a BS and a UAV [33]. Thus, in this paper, the UAVs are regarded as LoS targets for all BSs.[4] Specifically, the sensing link between the typical BS and the typical UAV can be modeled by the target response matrix $\mathbf{G}_{\mathbf{x},q,\mathbf{x}}$ as

$$\mathbf{G}_{\mathbf{x},q,\mathbf{x}} = \sqrt{N_{\mathrm{r}}N_{\mathrm{t}}L_{\mathrm{S},\mathbf{x},q,\mathbf{x}}}\beta_{\mathrm{S},\mathbf{x},q,\mathbf{x}}\mathbf{a}_{\mathrm{r}}(\phi_{\mathrm{S},\mathbf{x},q}, \theta_{\mathrm{S},\mathbf{x},q})\mathbf{a}^{\mathrm{H}}_{\mathrm{t}}(\phi_{\mathrm{S},\mathbf{x},q}, \theta_{\mathrm{S},\mathbf{x},q}), \tag{13}$$

where $\beta_{\mathrm{S},\mathbf{x},q,\mathbf{x}}$ is the Nakagami fading of the round-trip link between the typical BS $\mathbf{x}$ and the typical UAV with $\beta^2_{\mathrm{S},\mathbf{x},q,\mathbf{x}} \sim \mathrm{Gamma}(m_{\mathrm{L}}, m_{\mathrm{L}})$, and $L_{\mathrm{S},\mathbf{x},q,\mathbf{x}} = \frac{\bar{\sigma}}{4\pi}\zeta(r_0^2 + \Delta H^2)^{-\alpha_{\mathrm{L}}}$ is the round-trip path loss between $\mathbf{x}$ and the typical UAV, containing both the attenuation and radar cross section $\bar{\sigma}$ of UAVs.

The echo signal received at the typical BS, transmitted by itself and reflected by the typical UAV, is then modeled by

$$\mathbf{Y}_{\mathrm{S},\mathbf{x},q} = \mathbf{G}_{\mathbf{x},q,\mathbf{x}}\mathbf{X} + \mathbf{Z}_{\mathrm{S},\mathbf{x},q}, \tag{14}$$

where $\mathbf{Z}_{\mathrm{S},\mathbf{x},q} \in \mathbb{C}^{N_{\mathrm{r}}\times T}$ is the AWGN matrix of sensing links with each entry following CSCG distribution of variance $\sigma_{\mathrm{S}}B$ and σ_{S} being the noise power spectral density of sensing links.

IV. Standalone and Cooperative Sensing

In this section, we study both the standalone and cooperative sensing for UAV surveillance of the mmWave PMN, and propose a cooperative sensing strategy with the hybrid of monostatic sensing and bistatic sensing processes.

A. Network Clutter under Standalone Sensing

In PMNs, the sensing processes of BSs suffer from both the background clutter and the network clutter. Due to the low correlation with target echoes and the near-zero Doppler frequency, the background clutter generated by the static objects in background environment, such as ground, walls, trees, and mountains, can be removed by advanced clutter suppression algorithms such as the space-time adaptive processing [9]. On the other hand, a BS in PMNs also suffers from the network clutter that is transmitted by neighboring interfering BSs and reflected by wide-area UAVs, which has similar signal features to the desired echo and thus is difficult to eliminate [1]. The network clutter received by the typical BS from the direction of the typical UAV exerts major impacts on the desired echo, owing to the directional gain of antenna arrays. In general, the network clutter received by the typical BS for sensing the typical UAV under standalone sensing can be divided into four cases as illustrated in Fig. 2:

Case 1: If there exists another target UAV j of the typical BS, $j \neq q$, $j \in \{1, 2, \ldots, Q\}$, located in the same quantized virtual angle as the typical UAV q relative to the typical BS, then multi-target clutter will be caused between the echoes from UAV q and UAV j.

[3]Here, we assume that precise beam alignment between BSs and GUEs/UAVs is realized by the initial beam management phase [29].

[4]The sensing for NLoS targets can be achieved by advanced technologies with high computational complexity, such as intelligent reflecting surface [34], which is beyond the scope of this paper.

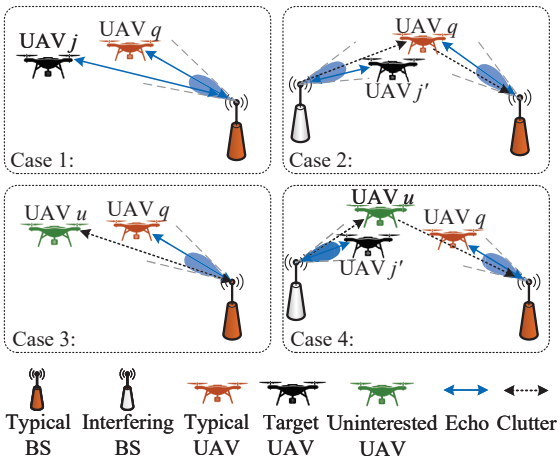

Fig. 2: Illustration of network clutter under standalone sensing.

Case 2: Besides the signal of the typical BS, the typical UAV also reflects back the transmit signals from the interfering BSs that have target UAVs located in the same quantized virtual angle as the typical UAV. Without cooperation, the signals from interfering BSs are unknown to the typical BS and cannot be utilized for echo extraction, thus being regarded as clutter.

Case 3: Except for the target UAV j stated in Case 1, there may also exist other uninterested UAVs, which are not one of the Q target UAVs of the typical BS but located in the same quantized virtual angle as the typical UAV q relative to the typical BS, thus can reflect back undesired network clutter.

Case 4: In addition, the uninterested UAVs also reflect the signals transmitted from the interfering BSs that have target UAVs in the directions of the uninterested UAVs.

B. Cooperative Sensing Strategy

To cope with the network clutter caused by neighboring interfering BSs, we propose a cooperative sensing strategy for PMNs based on the hybrid of monostatic sensing and bistatic sensing. Specifically, considering that the BSs close to the typical UAV will generate strong interference to the desired echo, we resort to a V-nearest-BSs cooperative policy. That is, the V nearest BSs to the typical UAV are selected to assist the typical BS in jointly sensing the typical UAV. The joint PDF of the horizontal distances between cooperative BSs and the typical UAV can be given by

$$f_V^{\mathrm{co}}(r_1, r_2, \ldots, r_V) = (2\pi\lambda_{\mathrm{b}})^V r_1 r_2 \cdots r_V \exp\big(-\pi\lambda_{\mathrm{b}} r_V^2\big), \tag{15}$$

which comes from the Bayes' theorem and the empty space probability of HPPP, $r_1 \le r_2 \le \cdots \le r_V$, and $r_v, v = 1, 2, \ldots, V$ is the horizontal distance between the v^{th}-nearest cooperative BS $\mathbf{x}_v$ and the typical UAV.

Given the V selected cooperative BSs, the detailed cooperative sensing procedure is explained as follows: First, the V cooperative BSs share their own ISAC transmit signals to the typical BS through fiber links. Then, the typical BS transmits its ISAC signal to the typical UAV and receives echo signal via monostatic sensing process. The V cooperative BSs also send their ISAC signals to the typical UAV, while the V echo signals are received by the typical BS via bistatic sensing processes. Thanks to the acquisition of the ISAC transmit signals of cooperative BSs, the V echo signals from the typical UAV transmitted by the cooperative BSs are no longer clutter signals to the typical BS, but turn into useful echo signals containing target information. Therefore, the proposed cooperative sensing strategy not only reduces the network clutter but also enhances the desired echo by virtue of the spatial diversity from multiple BSs. Similar to (14), the total received echo at the typical BS with V cooperative BSs can be given as

$$\mathbf{Y}_{\mathrm{S},\mathbf{x},q}^{(V)} = \mathbf{G}_{\mathbf{x},q,\mathbf{x}}\mathbf{X} + \sum\nolimits_{v=1}^{V} \mathbf{G}_{\mathbf{x}_v,q,\mathbf{x}}\mathbf{X}_v + \mathbf{Z}_{\mathrm{S},\mathbf{x},q}, \tag{16}$$

where $\mathbf{G}_{\mathbf{x}_v,q,\mathbf{x}}$ is the target response matrix of the bistatic sensing link from the v^{th} cooperative BS $\mathbf{x}_v$ to the typical UAV q and then to the typical BS $\mathbf{x}$, and $\mathbf{X}_v, v = 1, 2, \ldots, V$ is the ISAC transmit signal of the v^{th} cooperative BS.

V. Performance Analysis

In this section, by leveraging stochastic geometry, we conduct system-level analyses for communication and sensing performance in both standalone and cooperative sensing cases.

A. Rate Coverage Probability

In this subsection, to study how the added sensing function influences the communication performance in PMNs, we analyze the RCP for downlink communications.

Definition 1 (RCP): The RCP P_{rate} is defined as the probability that the downlink rate of the typical GUE is no less than a certain threshold, and is expressed as $P_{\mathrm{rate}} = \sum_{K_0=1}^{\infty} \frac{\mathbb{P}(K_{\mathrm{G}}=K_0)}{1-\mathbb{P}(K_{\mathrm{G}}=0)} P_{\mathrm{rate},K_0}$. Here, P_{rate,K_0} is the RCP of the typical GUE conditioned on K_0 GUEs in the coverage area of the typical BS, given by

$$P_{\mathrm{rate},K_0} = \mathbb{P}\Big[\frac{K}{K_0} B \log_2(1 + \mathrm{SINR}_{K,k}) \ge \tau_{\mathrm{C}}\Big], \tag{17}$$

where $\mathrm{SINR}_{K,k}$ is the signal-to-interference-plus-noise ratio (SINR) received by the typical GUE k, K is the number of associated GUEs of the typical BS, equal to K_0 if $K_0 \le K_{\max}$ and $K_{\max}$ if $K_0 > K_{\max}$, $\frac{K}{K_0}$ is the average scheduling probability of the typical GUE associated with the typical BS,[5] and τ_{C} is the rate threshold.

Due to the co-time co-frequency transmissions from BSs to GUEs, the intra-cell and inter-cell interference in downlink communications should be considered. In addition, the dedicated sensing symbols contain no useful information for GUEs, which are also seen as interference signals. Thus, the SINR at the typical GUE, $\mathrm{SINR}_{K,k}$, is given as

$$\mathrm{SINR}_{K,k} = \frac{\big\|\mathbf{h}_{\mathbf{x},k}^{\mathrm{H}} \mathbf{w}_{\mathrm{C},\mathbf{x},k} \mathbf{s}_{\mathrm{C},\mathbf{x},k}\big\|^2}{I_{\mathrm{intra,C}} + I_{\mathrm{intra,S}} + I_{\mathrm{inter}} + T\sigma_{\mathrm{C}} B}, \tag{18}$$

[5]Note that $\frac{K}{K_0}$ also captures the average scheduling probability under round-robin scheduling policy. Other scheduling policies can also be adopted for the PMN and modeled herein by modifying the scheduling probability accordingly [35].

where $I_{\text{intra,C}} = \sum_{i=1,i\neq k}^{K} \left\| \mathbf{h}_{\mathbf{x},k}^{\text{H}} \mathbf{w}_{\text{C},\mathbf{x},i} \mathbf{s}_{\text{C},\mathbf{x},i} \right\|^2$ is the multi-user interference caused by the communication symbols for the other $(K-1)$ associated GUEs; $I_{\text{intra,S}} = \mathbf{1}(Q \neq 0) \sum_{j=1}^{Q} \left\| \mathbf{h}_{\mathbf{x},k}^{\text{H}} \mathbf{w}_{\text{S},\mathbf{x},j} \mathbf{s}_{\text{S},\mathbf{x},j} \right\|^2$ is the intra-cell interference caused by the sensing symbols for the Q target UAVs; and I_{inter} is the inter-cell interference caused by the ISAC signals transmitted by interfering BSs, satisfying

$$I_{\text{inter}} = \sum_{K_0'=1}^{\infty} \sum_{\mathbf{x}' \in \Phi_{\text{B}}^{(K_0')} \setminus \mathbf{x}} \Big(\sum_{i'=1}^{K'} \left\| \mathbf{h}_{\mathbf{x}',k}^{\text{H}} \mathbf{w}_{\text{C},\mathbf{x}',i'} \cdot \mathbf{s}_{\text{C},\mathbf{x}',i'} \right\|^2 + \sum_{j'=1}^{Q'} \left\| \mathbf{h}_{\mathbf{x}',k}^{\text{H}} \mathbf{w}_{\text{S},\mathbf{x}',j'} \mathbf{s}_{\text{S},\mathbf{x}',j'} \right\|^2 \Big). \tag{19}$$

Here, $\Phi_{\text{B}}^{(K_0')}$ is the set of interfering BSs of density $\mathbb{P}(K_{\text{G}} = K_0')\lambda_{\text{b}}$ and with K_0' GUEs in the coverage area of each BS; $\mathbf{h}_{\mathbf{x}',k}$ is the channel vector of the link from the interfering BS $\mathbf{x}'$ to the typical GUE k, depending on the Nakagami fading and path loss; $K' = \min\{K_0', K_{\max}\}$ and $Q' = \min\{Q_0', Q_{\max}\}$ are the numbers of associated GUEs and target UAVs of the interfering BS $\mathbf{x}'$, respectively, with their quantized virtual angles relative to $\mathbf{x}'$ being the independent and identically distributed random variables following the PMF given in (7); Q_0' is the number of UAVs within the sensing area of BS $\mathbf{x}'$; $\mathbf{w}_{\text{C},\mathbf{x}',i'}$ and $\mathbf{w}_{\text{S},\mathbf{x}',j'}$ are the transmit beamforming vectors of $\mathbf{x}'$ for its i'^{th} associated GUE and j'^{th} target UAV, respectively; and $\mathbf{s}_{\text{C},\mathbf{x}',i'}$ and $\mathbf{s}_{\text{S},\mathbf{x}',j'}$ are the communication and sensing transmit symbols of $\mathbf{x}'$ for its i'^{th} associated GUE and j'^{th} target UAV, respectively.

Based on stochastic geometry, the RCP for downlink communications in PMNs is given in the following theorem.

Theorem 1: For the mmWave PMN, the RCP of the typical GUE conditioned on K_0 GUEs in the coverage area of the typical BS, P_{rate,K_0}, is derived as

$$P_{\text{rate},K_0} = \mathbb{E}_Q \mathbb{E}_{\delta_{k,i}} \Bigg\{ \int_0^{\infty} \sum_{e\in\{\text{L,N}\}} \mathbb{P}_e(v_0) \sum_{c=0}^{m_e-1} \frac{s_e^c}{c!} \exp(-s_e \sigma_{\text{C}} B) \sum_{l=0}^{c} \binom{c}{l} (-1)^{2c-l} (\sigma_{\text{C}} B)^{(c-l)} \frac{\mathrm{d}^l \mathcal{L}_{I_{\text{inter}}}(s_e)}{\mathrm{d}s_e^l} \mathbf{1}(s_e > 0) f_{\text{G}}(v_0) \mathrm{d}v_0 \Bigg\} \tag{20}$$

where $s_e = m_e \tau_{\text{C},K_0} \zeta^{-1} N_{\text{t}}^{-1} \big\{ \frac{P_{\text{t,C}}}{K} G_{\text{t}}^2 - \tau_{\text{C},K_0} \frac{P_{\text{t,C}}}{K} \sum_{i=1,i\neq k}^{K} [\delta_{k,i} G_{\text{t}}^2 + (1-\delta_{k,i}) g_{\text{t}}^2] - \tau_{\text{C},K_0} P_{\text{t,S}} g_{\text{t}}^2 \mathbf{1}(Q \neq 0) \big\}^{-1} (v_0^2 + H_{\text{B}}^2)^{\frac{\alpha_e}{2}}$, $e \in \{\text{L,N}\}$ and $\tau_{\text{C},K_0} = \exp[\tau_{\text{C}} K_0 \ln 2/(BK)] - 1$; $\delta_{k,i}$ is an indicator variable representing whether the i^{th}, $i = 1,2,\ldots,K$, $i \neq k$ associated GUE is in the same quantized virtual azimuth and elevation angles as the typical GUE k relative to the typical BS $\mathbf{x}$, equal to 1 with probability $\sum_{m=1}^{N_{\text{t,az}}} \sum_{n=1}^{N_{\text{t,el}}} {p_{\text{C,t}}^{(\text{ty})}}^2(\phi_m, \theta_n)$ and 0 otherwise; and $\mathcal{L}_{I_{\text{inter}}}(s_e)$ is the Laplace transform of the inter-cell interference given in (21) shown at the bottom of this page. Particularly, the derivation term $\frac{\mathrm{d}^l \mathcal{L}_{I_{\text{inter}}}(s_e)}{\mathrm{d}s_e^l}$ in (20) is recast as $\mathcal{L}_{I_{\text{inter}}}(s_e)$ when $l = 0$.

Proof: Please see Appendix B. □

Remark 1: The RCP is determined by the proportions of transmit power and RF chain resources allocated for communication, ρ and η, respectively, as well as the densities of BSs and GUEs, λ_{b} and λ_{g}, respectively. Note that Theorem 1 is also suitable for analyzing the RCP performance of communication-only mmWave cellular networks, by setting $\rho = \eta = 1$.

In (21), ${}_2F_1()$ is the Gaussian hypergeometric function, $\xi_1 = N_{\text{t}} \zeta \big\{ \frac{P_{\text{t,C}}}{K'} \sum_{i'=1}^{K'} \big[\delta_{k,i'} G_{\text{t}}^2 + (1-\delta_{k,i'}) g_{\text{t}}^2 \big] + P_{\text{t,S}} g_{\text{t}}^2 \mathbf{1}(Q' \neq 0) \big\}$, and $\delta_{k,i'}, i' = 1,2,\ldots,K'$ is an indicator variable denoting whether the i'^{th} associated GUE of the interfering BS $\mathbf{x}'$ is in the same quantized virtual angle as the typical GUE relative to $\mathbf{x}'$, equal to 1 with probability $\sum_{m=1}^{N_{\text{t,az}}} \sum_{n=1}^{N_{\text{t,el}}} p_{\text{C,t}}^{(\text{ty})}(\phi_m, \theta_n) p_{\text{C,t}}^{(\text{ar})}(\phi_m, \theta_n)$ and 0 otherwise.

Remark 2: Note that the numerical calculations for the infinite integrals and Gaussian hypergeometric functions in the above theorem by MATLAB are based on the discretization for infinite integral intervals and the truncation for infinite summations, which may lead to minor numerical errors [36]. At the cost of increased computational overhead, the numerical errors can be reduced by constraining the minimal tolerable precision. Moreover, the computational complexity for (20) stemming from the calculation of the infinite integral terms and special functions can be given as $\mathcal{O}(WS \log S)$ [37], where S and W are respectively the number of the discrete segments of the integral interval in (20) and the number of the summation terms to approximate the Gaussian hypergeometric function in (21) and can be considered as the complexity-vs-accuracy tradeoff parameters [36, 37].

B. Successful Detection Probability under Standalone Sensing

In this subsection, we study the SDP under standalone sensing for PMNs considering the complex network clutter. We first give the definition of SDP, which is used in both standalone and cooperative sensing cases.

Definition 2 (SDP): The SDP for UAVs in standalone and cooperative sensing cases, P_{det}^{κ}, is defined as the probability that the typical UAV can be successfully detected by the typical BS, and is expressed as $P_{\text{det}}^{\kappa} = \sum_{Q_0=1}^{\infty} \frac{\mathbb{P}(Q_{\text{U}}=Q_0)}{1-\mathbb{P}(Q_{\text{U}}=0)} P_{\text{det},Q_0}^{\kappa}$. Here, $P_{\text{det},Q_0}^{\kappa}$ is the SDP conditioned on Q_0 UAVs in the sensing area of the typical BS, given by

$$P_{\text{det},Q_0}^{\kappa} = \frac{Q}{Q_0} \mathbb{P}(\text{SCNR}_{Q,q}^{\kappa} \geq \tau_{\text{S}}), \tag{22}$$

where $\kappa \in \{\text{st}, \text{co}\}$ stands for "standalone" or "cooperative" sensing, $\text{SCNR}_{Q,q}^{\kappa}$ is the signal-to-clutter-plus-noise ratio (SCNR) received at the typical BS for sensing the typical UAV q and is analyzed in further detail below, Q is the number of target UAVs of the typical BS and $Q = \min\{Q_0, Q_{\max}\}$, Q/Q_0 is the scheduling probability that a UAV in the sensing area of the typical BS can be selected as a target UAV, and τ_{S} is the SCNR threshold that a BS requires to successfully acquire target information from echo signals.

Remark 3: SCNR is widely used to measure the ability of clutter suppression and echo extraction [14]. Increasing SCNR has great significance for the reduction of false alarm probability and the improvement of target detection performance in radar fields. Thus, similar to [14], the SDP based on SCNR is adopted for performance evaluation in this paper.

Next, we present the definition of sensing outage probability to evaluate the sensing coverage capability of the PMN.

Definition 3 (SOP): The SOP for the UAV surveillance-oriented PMN in standalone and cooperative sensing cases, $P_{\text{out}}^{\kappa}, \kappa \in \{\text{st}, \text{co}\}$, is defined as the probability that a UAV cannot be successfully detected by BSs, given by

$$P_{\text{out}}^{\kappa} = U_{\text{out}} + (1 - U_{\text{out}})(1 - P_{\text{det}}^{\kappa}), \tag{23}$$

where $U_{\text{out}} = \exp(-\pi\lambda_{\text{b}} R_{\text{S}}^2)$ is the probability that a UAV is out of surveillance by any of the BSs and is derived from the empty space probability of HPPP.

Remark 4: The SOP is affected by not only the SDP performance but also the sensing distance and deployment density of BSs. Both the SDP and SOP are highly determined by the received SCNR. In particular, in an ideal scenario with all BSs having the sensing area of the whole network (i.e., $U_{\text{out}} = 0$), $P_{\text{out}}^{\kappa} = 1 - P_{\text{det}}^{\kappa}$ holds true, leading to the sensing coverage capability in this case only dependent on the successful detection performance.

Different from downlink communication, in UAV detection processes, the communication symbols can be regarded as useful symbols for target sensing without causing any extra interference. This is because the target information depends on the amplitude and phase changes of signals instead of the specific data symbols [14]. The simultaneous sensing for Q target UAVs would cause mutual interference among Q target echoes. With the analog receive beamforming [3], the SCNR received at the typical BS for sensing the typical UAV q under standalone sensing, $\text{SCNR}_{Q,q}^{\text{st}}$, can be expressed as

$$\text{SCNR}_{Q,q}^{\text{st}} = \frac{\left\|\mathbf{a}_{\text{r}}^{\text{H}}(\phi_{\text{S},\mathbf{x},q}, \theta_{\text{S},\mathbf{x},q})\mathbf{G}_{\mathbf{x},q,\mathbf{x}}\mathbf{X}\right\|^2}{C_{\mathbf{x},q}^{\text{st}} + T\sigma_{\text{S}}B}, \tag{24}$$

where $\mathbf{a}_{\text{r}}(\phi_{\text{S},\mathbf{x},q}, \theta_{\text{S},\mathbf{x},q})$ is the directional receive beamforming vector for the echo from the typical UAV q, $C_{\mathbf{x},q}^{\text{st}}$ is the network clutter that interferes with the target echo in the standalone sensing case, and it can be expressed based on the four cases elaborated in Subsection IV-A as:

$$\begin{aligned} C_{\mathbf{x},q}^{\text{st}} = &\underbrace{\sum\nolimits_{j=1,j\neq q}^{Q} \delta_{q,j}\left\|\mathbf{a}_{\text{r}}^{\text{H}}(\phi_{\text{S},\mathbf{x},q},\theta_{\text{S},\mathbf{x},q})\mathbf{G}_{\mathbf{x},j,\mathbf{x}}\mathbf{X}\right\|^2}_{C_{\mathbf{x},q}^{(1)}} + \underbrace{\sum\nolimits_{\mathbf{x}'\in\Phi_{\text{B}}^{(q)}\setminus\mathbf{x}}}_{C_{\mathbf{x},q}^{(2)}} \\ &\underbrace{\left\|\mathbf{a}_{\text{r}}^{\text{H}}(\phi_{\text{S},\mathbf{x},q},\theta_{\text{S},\mathbf{x},q})\mathbf{G}_{\mathbf{x}',q,\mathbf{x}}\mathbf{X}'\right\|^2}_{C_{\mathbf{x},q}^{(2)}} + \underbrace{\sum\nolimits_{u\in\Phi_{\text{U}}^{(q)}\setminus q}\left\|\mathbf{a}_{\text{r}}^{\text{H}}(\phi_{\text{S},\mathbf{x},q},\theta_{\text{S},\mathbf{x},q})\right.}_{C_{\mathbf{x},q}^{(3)}} \cdot \\ &\underbrace{\left\|\mathbf{G}_{\mathbf{x},u,\mathbf{x}}\mathbf{X}\right\|^2}_{C_{\mathbf{x},q}^{(3)}} + \underbrace{\sum\nolimits_{u\in\Phi_{\text{U}}^{(q)}\setminus q}\left\|\mathbf{a}_{\text{r}}^{\text{H}}(\phi_{\text{S},\mathbf{x},q},\theta_{\text{S},\mathbf{x},q})\mathbf{G}_{\mathbf{x}'_{\text{n}},u,\mathbf{x}}\mathbf{X}'_{\text{n}}\right\|^2}_{C_{\mathbf{x},q}^{(4)}}. \end{aligned} \tag{25}$$

Here, $\delta_{q,j}$ is the indicator variable that represents whether the j^{th} target UAV is in the same quantized virtual angle as the typical UAV q, equal to 1 with probability $p_{\text{main,S},1} = \sum_{m=1}^{N_{\text{t,az}}}\sum_{n=1}^{N_{\text{t,el}}} {p_{\text{S,t}}^{(\text{ty})}}^2(\phi_m, \theta_n)$ and 0 otherwise. $\Phi_{\text{B}}^{(q)}$ is the set of interfering BSs with at least one target UAV $j', j' \in \{1, 2, \ldots, Q'\}$ located in the same quantized virtual angle as the typical UAV q, and whether the target UAV j' of $\mathbf{x}'$ is in the same quantized virtual angle as the typical UAV relative to $\mathbf{x}'$ is denoted by an indicator variable $\delta_{q,j'}$, equal to 1 with probability $p_{\text{main,S},2} = \sum_{m=1}^{N_{\text{t,az}}}\sum_{n=1}^{N_{\text{t,el}}} p_{\text{S,t}}^{(\text{ty})}(\phi_m, \theta_n) p_{\text{S,t}}^{(\text{ar})}(\phi_m, \theta_n)$ and 0 otherwise. $\Phi_{\text{U}}^{(q)}$ is the set of uninterested UAVs that are in the same quantized virtual angle as the typical UAV relative to $\mathbf{x}$ with density $p_{\text{main,S},2}\lambda_{\text{u}}$. $\mathbf{X}'$ is the transmit signal matrix of the interfering BS $\mathbf{x}'$ and can be similarly given as (8). $\mathbf{G}_{\mathbf{x}',q,\mathbf{x}}$ and $\mathbf{G}_{\mathbf{x},u,\mathbf{x}}$ are the target response matrices of the sensing links from the interfering BS to the typical UAV and then to the typical BS, and from the typical BS to the uninterested UAV u and then back to the typical BS, respectively. Additionally, for analytical tractability, in term $C_{\mathbf{x},q}^{(4)}$ only the interfering BS $\mathbf{x}'_{\text{n}}$ that generates the strongest clutter link to the uninterested UAV u is considered [38, 39]. $\mathbf{G}_{\mathbf{x}'_{\text{n}},u,\mathbf{x}}$ is the target response matrix of the sensing link from the interfering BS $\mathbf{x}'_{\text{n}}$ to u and then to the typical BS, and $\mathbf{X}'_{\text{n}}$ is the transmit signal matrix of this interfering BS.

Based on stochastic geometry, the SDP in the standalone sensing case is given by the following theorem.

Theorem 2: For the mmWave PMN, the SDP for sensing the typical UAV by the typical BS conditioned on Q_0 UAVs in its sensing area, $P_{\text{det},Q_0}^{\text{st}}$, is derived as

$$\begin{aligned} P_{\text{det},Q_0}^{\text{st}} = \mathbb{E}_K\mathbb{E}_{\delta_{q,j}}\Bigg\{\frac{Q}{Q_0}\int_0^{R_{\text{S}}}\sum_{c=0}^{m_{\text{L}}-1}\frac{s_{\text{S}}^c}{c!}\exp(-s_{\text{S}}\sigma_{\text{S}}B)\sum_{l=0}^{c} \\ (-1)^{2c-l}\tbinom{c}{l}(\sigma_{\text{S}}B)^{c-l}\frac{\mathrm{d}^l\mathcal{L}_{C_{\mathbf{x},q}^{\text{st}}}(s_{\text{S}})}{\mathrm{d}s_{\text{S}}^l}f_{\text{U}}(r_0)\mathrm{d}r_0\Bigg\}, \end{aligned} \tag{26}$$

where $s_{\text{S}} = m_{\text{L}}\tau_{\text{S}}\big\{G_{\text{r}}^2 N_{\text{r}} N_{\text{t}}\frac{\bar{\sigma}}{4\pi}\zeta\big\{P_{\text{t,C}}g_{\text{t}}^2\mathbf{1}(K\neq 0) + \frac{P_{\text{t,S}}}{Q}G_{\text{t}}^2 + \sum_{j=1,j\neq q}^{Q}\frac{P_{\text{t,S}}}{Q}[\delta_{q,j}G_{\text{t}}^2 + (1-\delta_{q,j})g_{\text{t}}^2]\big\}(r_0^2 + \Delta H^2)^{-\alpha_{\text{L}}}\big\}^{-1}$, and the Laplace transform of network clutter $\mathcal{L}_{C_{\mathbf{x},q}^{\text{st}}}(s_{\text{S}})$ equals the product of $\mathcal{L}_{C_{\mathbf{x},q}^{(1)}}(s_{\text{S}})$, $\mathcal{L}_{C_{\mathbf{x},q}^{(2)}}(s_{\text{S}})$, $\mathcal{L}_{C_{\mathbf{x},q}^{(3)}}(s_{\text{S}})$, and $\mathcal{L}_{C_{\mathbf{x},q}^{(4)}}(s_{\text{S}})$ given in (39)-(42), respectively.

Proof: Please see Appendix C. □

Remark 5: The SDP is influenced by the power allocation coefficient ρ and the number of target UAVs Q. It is noteworthy that Q is inherently dependent on the proportion of RF chains allocated for sensing $1-\eta$, BS density λ_{b}, UAV density λ_{u}, and sensing distance of BSs R_{S}.

Remark 6: With all the BSs possessed of dual-functional capability, Theorem 2 provides the worst-case SDP of PMNs, given the severe network clutter caused by the large-scale

$$\begin{aligned} \mathcal{L}_{I_{\text{inter}}}(s_e) = \prod_{K_0'=1}^{\infty}\prod_{e'\in\{\text{L},\text{N}\}}\exp\Bigg\{\frac{2\pi}{\alpha_{e'}}\mathbb{P}(K_{\text{G}}=K_0')\lambda_{\text{b}}\frac{\int_0^{\infty}\mathbb{P}_{\text{L}}(v)v\mathrm{d}v}{\int_0^{\infty}v\mathrm{d}v}\mathbb{E}_{Q'}\mathbb{E}_{\delta_{k,i'}}\Bigg\{\sum_{t=1}^{m_{e'}}\tbinom{m_{e'}}{t}(-1)^t\frac{s_e^t\xi_1^t(v_0^2+H_{\text{B}}^2)^{1-\frac{\alpha_{e'}t}{2}}}{(t-\frac{2}{\alpha_{e'}})m_{e'}^t}\cdot \\ {}_2F_1\Big(t, t-\tfrac{2}{\alpha_{e'}}; t-\tfrac{2}{\alpha_{e'}}+1; -\frac{\xi_1 s_e}{m_{e'}(v_0^2+H_{\text{B}}^2)^{\frac{\alpha_{e'}}{2}}}\Big)\Bigg\}\Bigg\}. \end{aligned} \tag{21}$$

interfering BSs. Theorem 2 is also applicable for the sensing performance of heterogeneous PMNs where dual-functional BSs and communication-only BSs coexist, by setting $\lambda_{\rm b}$ in (26) to $p\lambda_{\rm b}$, with p being the proportion of the number of dual-functional BSs to the total number of BSs.

Combining (5), (23), and (26), the SOP for the mmWave UAV surveillance-oriented PMN in the standalone sensing case, $P_{\rm out}^{\rm st}$, can be expressed as

$$P_{\rm out}^{\rm st}=U_{\rm out}+(1-U_{\rm out})\bigg[1-\sum_{Q_0=1}^{\infty}\frac{\mathbb{P}(Q_{\rm U}=Q_0)}{1-\mathbb{P}(Q_{\rm U}=0)}P_{{\rm det},Q_0}^{\rm st}\bigg]. \tag{27}$$

C. SDP under Cooperative Sensing

As elaborated in Section IV-B, with the collaboration of V cooperative BSs, the proposed cooperative sensing strategy can enhance the useful echo and reduce clutter compared with standalone sensing. The SCNR received at the typical BS for sensing the typical UAV via the hybrid of monostatic sensing and bistatic sensing is given by

$$\mathrm{SCNR}_{Q,q}^{\rm co}=\frac{\Big\|\mathbf{a}_{\rm r}^{\rm H}(\phi_{{\rm S},\mathbf{x},q},\theta_{{\rm S},\mathbf{x},q})\big(\mathbf{G}_{\mathbf{x},q,\mathbf{x}}\mathbf{X}+\sum_{v=1}^{V}\mathbf{G}_{\mathbf{x}_v,q,\mathbf{x}}\mathbf{X}_v\big)\Big\|^2}{C_{\mathbf{x},q}^{\rm co}+T\sigma_{\rm S}B}, \tag{28}$$

where $C_{\mathbf{x},q}^{\rm co}$ is the network clutter in the cooperative sensing case and can be obtained similar to $C_{\mathbf{x},q}^{\rm st}$ given in (25) but excluding the clutter caused by the V cooperative BSs, expressed as

$$C_{\mathbf{x},q}^{\rm co}=C_{\mathbf{x},q}^{(1)}+\sum_{\substack{\mathbf{x}'\in\Phi_{\rm B}^{(q)}\setminus\\ \{\mathbf{x},\mathbf{x}_1,\ldots,\mathbf{x}_V\}}}\big\|\mathbf{a}_{\rm r}^{\rm H}(\phi_{{\rm S},\mathbf{x},q},\theta_{{\rm S},\mathbf{x},q})\mathbf{G}_{\mathbf{x}',q,\mathbf{x}}\mathbf{X}'\big\|^2+C_{\mathbf{x},q}^{(3)}+C_{\mathbf{x},q}^{(4)}. \tag{29}$$

The randomness of the multiple target echoes under cooperative sensing as shown in (28) increases the difficulty of further analysis of SDP. Thus, the following lemma is given to facilitate the analysis by approximating the total power of multiple echoes as a Gamma random variable.

Lemma 1: (Approximation of the sum of Gamma random variables [40]) Let $\{\mathcal{G}_v\}_{v=1}^{V}$ be a set of independent Gamma variables with shape and rate parameters $\{\epsilon_v\}_{v=1}^{V}$ and $\{\mu_v\}_{v=1}^{V}$, respectively. The sum of V variables $\mathcal{G}=\sum_{v=1}^{V}\mathcal{G}_v$ can be approximated as a Gamma random variable, i.e., $\mathcal{G}\sim\Gamma(\tilde{\epsilon},\tilde{\mu})$, with $\tilde{\epsilon}=\frac{(\sum_{v=1}^{V}\frac{\epsilon_v}{\mu_v})^2}{\sum_{v=1}^{V}\frac{\epsilon_v}{\mu_v^2}}$ and $\tilde{\mu}=\frac{\sum_{v=1}^{V}\frac{\epsilon_v}{\mu_v}}{\sum_{v=1}^{V}\frac{\epsilon_v}{\mu_v^2}}$ being shape and rate parameters, respectively, which comes from the first and second order moments matching of $\mathcal{G}$ and $\sum_{v=1}^{V}\mathcal{G}_v$.

The approximated Gamma distribution obtained by Lemma 1 is generally with non-integral parameters $\tilde{\epsilon}$ and $\tilde{\mu}$, and thus it is still intractable to acquire a closed-form solution to the SDP performance under cooperative sensing. To this end, we resort to the Alzer's inequality to obtain a tight upper bound of SDP under cooperative sensing, which can be proven of good accuracy by simulations in Section VII.

Theorem 3: For the mmWave PMN, given V cooperative BSs and Q_0 UAVs in the sensing area of the typical BS, the upper bound of the SDP for sensing the typical UAV under cooperative sensing, $P_{{\rm det},Q_0}^{\rm co}$, can be obtained by

$$\begin{aligned}P_{{\rm det},Q_0}^{\rm co}<\frac{Q}{Q_0}\Bigg\{1-\sum_{z=0}^{\infty}\frac{(-1)^z}{z!}\mathbb{E}_{Q_{V,v}}\Bigg\{\int_0^{R_{\rm S}}\int_0^{\infty}\int_{r_1}^{\infty}\cdots\int_{r_{V-1}}^{\infty}\prod_{t=0}^{z-1}(\tilde{\epsilon}-t)\cdot\\ \exp\Big\{-z\big[\Gamma(1+\tilde{\epsilon})\big]^{-\frac{1}{\tilde{\epsilon}}}\tilde{\mu}\tau_{\rm S}\sigma_{\rm S}B\Big\}\mathcal{L}_{C_{\mathbf{x},q}^{\rm co}}\Big(z\big[\Gamma(1+\tilde{\epsilon})\big]^{-\frac{1}{\tilde{\epsilon}}}\tilde{\mu}\tau_{\rm S}\Big)\cdot\\ f_{\rm U}(r_0)f_V^{\rm co}(r_1,r_2,\cdots,r_V)\mathrm{d}r_V\mathrm{d}r_{V-1}\cdots\mathrm{d}r_0\Bigg\}\Bigg\},\end{aligned} \tag{30}$$

where $Q_{V,v}$ is the number of target UAVs of the $v^{\rm th}$ cooperative BS, the Laplace transform $\mathcal{L}_{C_{\mathbf{x},q}^{\rm co}}\big(z\big[\Gamma(1+\tilde{\epsilon})\big]^{-\frac{1}{\tilde{\epsilon}}}\tilde{\mu}\tau_{\rm S}\big)$ in (30) equals the product of equations (39)-(42) with the minimum horizontal distance between the interfering BSs and the typical UAV, $\nu_{\min}$ in (40), equal to r_V, and $\tilde{\epsilon}$ and $\tilde{\mu}$ can be obtained according to Lemma 1 as

$$\tilde{\epsilon}=\frac{m_{\rm L}\big(\mathcal{P}_0+\sum_{v=1}^{V}\mathcal{P}_v\big)^2}{\mathcal{P}_0^2+\sum_{v=1}^{V}\mathcal{P}_v^2},\ \tilde{\mu}=\frac{m_{\rm L}\big(\mathcal{P}_0+\sum_{v=1}^{V}\mathcal{P}_v\big)}{\mathcal{P}_0^2+\sum_{v=1}^{V}\mathcal{P}_v^2}, \tag{31}$$

where $\mathcal{P}_0=\zeta\frac{\bar{\sigma}}{4\pi}G_{\rm r}^2N_{\rm r}N_{\rm t}\Big\{P_{{\rm t,C}}g_{\rm t}^2\mathbf{1}(K\neq 0)+\frac{P_{\rm t,S}}{Q}G_{\rm t}^2+\sum_{j=1,j\neq q}^{Q}\frac{P_{\rm t,S}}{Q}[\delta_{q,j}G_{\rm t}^2+(1-\delta_{q,j})g_{\rm t}^2]\Big\}(r_0^2+\Delta H^2)^{-\alpha_{\rm L}}$ and $\mathcal{P}_v=\zeta\frac{\bar{\sigma}}{4\pi}G_{\rm r}^2N_{\rm r}N_{\rm t}\big[P_{{\rm t,C}}g_{\rm t}^2+\frac{P_{\rm t,S}}{Q_{V,v}}G_{\rm t}^2+\frac{P_{\rm t,S}(Q_{V,v}-1)}{Q_{V,v}}g_{\rm t}^2\big](r_0^2+\Delta H^2)^{-\frac{\alpha_{\rm L}}{2}}(r_v^2+\Delta H^2)^{-\frac{\alpha_{\rm L}}{2}}$.

Proof: Please see Appendix D. □

With the upper bound of SDP given in Theorem 3, the lower bound of SOP in the cooperative sensing case, $P_{\rm out}^{\rm co}$, can be given by definition as

$$P_{\rm out}^{\rm co}>U_{\rm out}+(1-U_{\rm out})\bigg[1-\sum_{Q_0=1}^{\infty}\frac{\mathbb{P}(Q_{\rm U}=Q_0)}{1-\mathbb{P}(Q_{\rm U}=0)}P_{{\rm det},Q_0}^{\rm co}\bigg]. \tag{32}$$

Remark 7: The premise of leveraging multiple sensing echoes to obtain the performance gain in SCNR is the acquisition of the original ISAC transmit signals of cooperative BSs at the typical BS, at the cost of extra backhaul overhead and larger total consumed power for UAV sensing.

From the above analyses on RCP, SDP, and SOP, the inherent interference of PMNs in terms of the multi-user and inter-cell communication interference, dual-functional mutual interference, and complex network clutter, and the resource contention between sensing and communication functions in terms of transmit power and RF chain resources are taken into account. By fine tuning network configurations based on the proposed theoretical framework, the inherent interference and resource contention of the UAV surveillance-oriented PMN can be appropriately controlled and the dual-functional performance tradeoff can be balanced, which contributes to the offline optimization for centralized network planning before practical deployments.

VI. Performance Optimization

In this section, to optimize network configurations, we study an optimization problem to improve the sensing performance of PMNs with the guarantee of communication demands.

As aforementioned, in mmWave UAV surveillance-oriented PMNs, the power allocation coefficient ρ, RF chain allocation coefficient η, BS density $\lambda_{\rm b}$, and sensing distance $R_{\rm S}$ are the key parameters that exert significant impacts on sensing and communication performance. Specifically, to better configure ρ, η, $\lambda_{\rm b}$, and $R_{\rm S}$, we formulate the following optimization problem to minimize the SOP under standalone and cooperative sensing whilst satisfying the requirements of RCP and SDP:

$$\begin{aligned} \min_{\rho,\eta,\lambda_{\rm b},R_{\rm S}} \quad & P_{\rm out}^{\kappa},\ \kappa\in\{\rm st,co\} \\ \text{s.t.} \quad & P_{\rm det}^{\kappa}\geq\varrho_{\rm S}, \\ & P_{\rm rate}\geq\varrho_{\rm C}, \end{aligned} \tag{33}$$

with $\varrho_{\rm S}$ and $\varrho_{\rm C}$ being the required SDP and RCP, respectively.[6] In view of the computational complexity of (20), (26), and (30), it is difficult to analytically obtain the global optimum. Therefore, we resort to the alternating optimization to address the problem [41]. To reduce algorithm complexity while maintaining good accuracy, inspired by the pyramid algorithm in image processing [42], we utilize a hierarchical search algorithm based on alternating optimization.

Specifically, considering the integral number of RF chains, η is discrete and takes all its possible values in the hierarchical search. The continuous parameters $\rho, \lambda_{\rm b}$, and $R_{\rm S}$ are all discretized into Ξ values, with Ξ taken the number of feasible values of η. The discrete granularity for the first search layer is set as $\delta_1 = \frac{\chi_{\max}-\chi_{\min}}{\Xi-1}$ and that for the $(n+1)^{\rm th}, n\geq 1$ layer is set as $\delta_{n+1} = \frac{\min\{\hat{\chi}^{(n)}+\delta_n,\chi_{\max}\}-\max\{\hat{\chi}^{(n)}-\delta_n,\chi_{\min}\}}{\Xi-1}$, $\hat{\chi}^{(n)}$ being the optimal value of $\chi\in\{\rho,\eta,\lambda_{\rm b},R_{\rm S}\}$ obtained in the $n^{\rm th}$ layer, and $[\chi_{\min},\chi_{\max}]$ being the feasible range of χ. In each search layer, on the premise of satisfying the required SDP and RCP, the four variables are alternately and iteratively optimized to minimize the SOP until convergence. That is, for each iteration, the variables are updated in turn, with the others fixed to the values obtained in the last iteration or updated in the current iteration. After convergence, the next search layer is conducted based on the same alternating optimization process. As the discrete granularity is adopted for the continuous variables, only a suboptimal solution to (33) can be obtained via the hierarchical search-based alternating optimization method. In addition, to find a good solution with controlled computational complexity, appropriately setting the number of initial values is important.

VII. Results and Discussions

In this section, we provide numerical and simulation results to investigate the dual-functional performance of UAV surveillance-oriented PMNs, where 1000 Monte Carlo simulations are conducted for each numerical result for validation with 5000×5000 m^2 simulation area. Unless otherwise stated, values of network parameters are given in Table I [9, 20, 22].

[6]Note that (33) can be treated as a long-term network performance optimization problem, of which the solution can be used as a reference for network configurations or a baseline for online adjustment. It can be solved at central units with strong computational and processing capabilities.

TABLE I: System Parameters

Parameter	Value	Parameter	Value
$\lambda_{\rm b}$	$2\times10^{-5}/\text{m}^2$	$\lambda_{\rm u}$	$2\times10^{-5}/\text{m}^2$
$\lambda_{\rm g}$	$2\times10^{-4}/\text{m}^2$	$H_{\rm B}, H_{\rm U}$	10 m, 60 m
$P_{\rm t}$	10 W	$N_{\rm RF,max}$	10
ρ,η	0.5, 0.5	$R_{\rm S}$	100 m
$N_w, w\in\{\rm t,r\}$	256	$N_{w,\rm az}, N_{w,\rm el}$	16, 16
f_c	28 GHz	B	100 MHz
$\sigma_{\rm C},\sigma_{\rm S}$	-174 dBm/Hz, -174 dBm/Hz	T	300
$\alpha_{\rm L},\alpha_{\rm N}$	2.5, 3.5	$m_{\rm L}, m_{\rm N}$	3, 1
G_w, g_w	$1, 0.27/N_w$	$\bar{\sigma}$	1 m^2
a, b	11.95, 0.136	$\tau_{\rm C},\tau_{\rm S}$	20 Mbps, 1

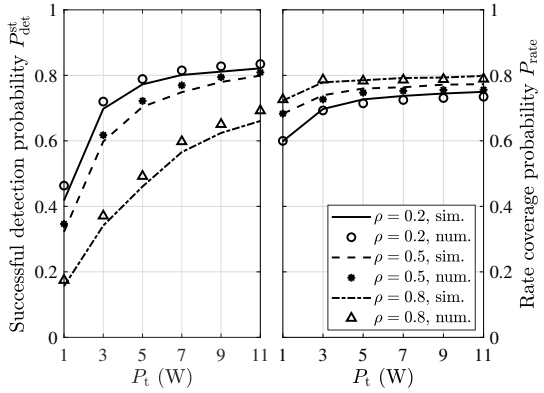

Fig. 3: SDP and RCP vs. total transmit power.

A. Performance of Communication and Standalone Sensing

To validate the theoretical analysis on dual-functional performance, Fig. 3 shows the numerical and simulation results on RCP and SDP in the standalone sensing case under different total transmit power $P_{\rm t}$ and power allocation coefficients ρ. The Monte Carlo simulation results match well with the numerical results.[7] As shown in Fig. 3, improving $P_{\rm t}$ can enhance both sensing and communication performance. However, the performance improvement slows down and tends to converge with the increase in $P_{\rm t}$. This is because, despite the enhancement of desired echoes and communication signals, a larger value of $P_{\rm t}$ also means stronger network clutter and communication interference in PMNs, thus restricting the improvement of the received SINR and SCNR. Moreover, the increase in $P_{\rm t}$ or the decrease in power allocation coefficient ρ brings remarkable performance enhancement in SDP, while the increase in the allocated transmit power for communication brings slight improvement in RCP. This is because, the round-trip transmission of target sensing experiences larger signal attenuation than the single-trip downlink communication, and thus is more vulnerable to power reduction. As a result, an appropriate setting of the total transmit power can effectively improve both sensing and communication performance. Also, taking into account the high power demand of sensing function, the power allocation between communication and sensing should be carefully tuned.

[7]Note that the discrepancy between numerical and simulation results on SDP stems from the numerical errors for calculating the round-trip sensing clutter with spatio-temporal randomness, which can be mitigated under scenarios with low BS/UAV density and high beamforming capability.

This article has been accepted for publication in IEEE Transactions on Wireless Communications. This is the author's version which has not been fully edited and content may change prior to final publication. Citation information: DOI 10.1109/TWC.2024.3488893

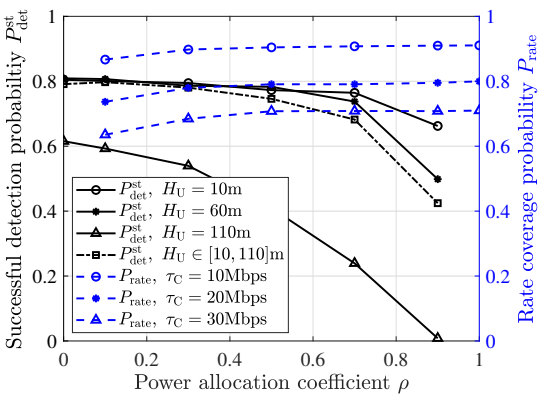

Fig. 4: SDP and RCP vs. power allocation coefficient.

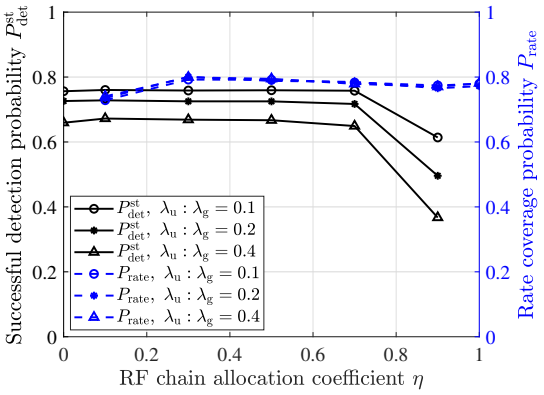

Fig. 5: SDP and RCP vs. RF chain allocation coefficient.

To further understand how the power sharing between sensing and communication affects their performance tradeoff, in Fig. 4, given the total transmit power, we present the relationships among the power allocation coefficient ρ, RCP, and SDP in the standalone sensing case. The simulation results show that ρ exerts opposite effects on sensing and communication performance. A large value of ρ causes low transmit power for sensing and leads to weak target echo and noticeably poor SDP, which in turn, brings strong communication power and improved RCP. In addition, a larger rate threshold $\tau_{\rm C}$ leads to lower RCP, owing to the higher requirement on communication. Furthermore, Fig. 4 also illustrates the sensing performance for UAVs at different altitudes. As UAVs fly high, the SDP declines sharply, especially when ρ is large. This is because the remarkable increase in transmission distances makes the sensing performance more vulnerable to power reduction and ambient noise. Moreover, it is noteworthy that the sensing performance for UAVs with uniformly distributed heights within $[10, 110]$ m is basically in consistent with that for the UAVs all at the mean height, 60 m. It implies that the proposed theoretical framework is also suitable for characterizing the network performance with 3D distributed UAVs, as observed in [17]. Overall, a large transmit power is required for sensing UAVs especially for the ones with high altitudes, and properly setting ρ can improve SDP under a satisfactory RCP.

In order to illustrate the dual-functional tradeoff under limited RF chain resources, in Fig. 5, considering different UAV densities $\lambda_{\rm u}$, we present the impacts of RF chain allocation coefficient η on RCP and SDP under standalone sensing. A larger η means that more RF chain resources are allocated to communication and less are reserved for sensing, thus resulting in poorer detection performance, especially when η equals 0.9. A small η can improve sensing capability, but it also leads to small transmit power allocated for sensing each UAV, thus restricting the enhancement of SDP. On the other hand, with the increase in η, the RCP increases first and then decreases. Similarly, too few RF chain resources for communication (e.g., $\eta = 0.1$) results in limited beamforming capability for communication and small RCP, while a large η leads to the reduction of the transmit power for each GUE. Particularly, as $\eta = 1$, there is a slight improvement in RCP compared with $\eta = 0.9$. This is because the mmWave PMN turns into a communication-only network when η equals 1, and without sensing function, the interference of sensing symbols to communication vanishes and the SINR is enhanced. Moreover, it is noteworthy from Fig. 5 that, the increase in UAV density $\lambda_{\rm u}$ causes performance degradation of SDP, but makes little difference in RCP. Although denser UAV aggravates the sensing load, the RF chain allocation coefficient η ensures the maximum capability of UAV surveillance by each BS, thus guaranteeing communication performance. In general, Fig. 5 gives important insights on the allocation of limited RF chain resource to enhance the dual-functional performance.

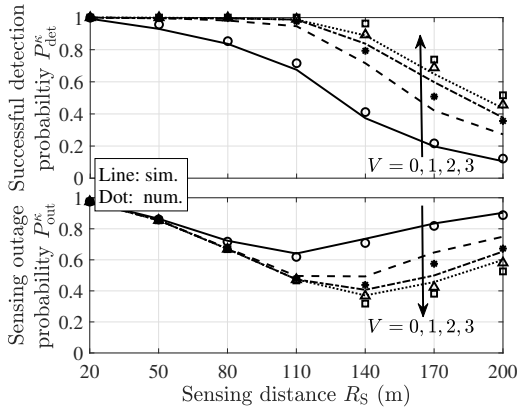

Fig. 6: SDP and SOP vs. sensing distance.

B. Performance of Communication and Cooperative Sensing

In Fig. 6, we present how the sensing distance $R_{\rm S}$ and number of cooperative BSs V affect the SDP and SOP in the cooperative sensing case. The numerical results from Theorem 3 are provided, as an upper bound of the SDP results obtained from Monte Carlo simulations. It can be observed that the SDP declines sharply with the increase of $R_{\rm S}$. This is rational because, the larger $R_{\rm S}$ means the farther distances between BSs and their target UAVs, resulting in weaker echo. Also, the target UAVs can be closer to nearby interfering BSs and suffer from severer clutter. In addition, with a larger $R_{\rm S}$, there exist more UAVs in the sensing areas of BSs, which reduces the power available for each UAV and the probability of being selected as target UAVs. On the other hand, the

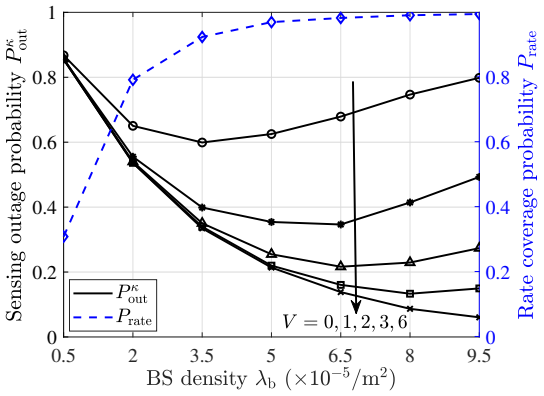

Fig. 7: SOP and RCP vs. BS density.

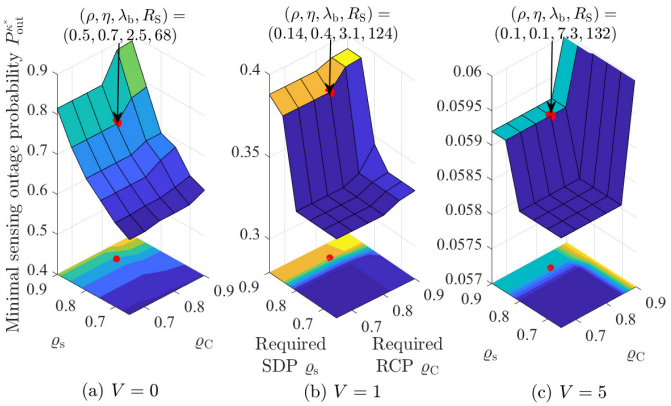

(a) $V = 0$ (b) $V = 1$ (c) $V = 5$

Fig. 8: Minimal SOP vs. required SDPs and RCPs.

SOP reaches the nadir and then rises with the increase in BS sensing distance. At first, the increase of R_{S} enlarges the sensing areas and reduces the proportion of UAVs that are out of the surveillance by BSs, thus leading to the decrease in SOP. However, the SOP deteriorates at a large R_{S}, due to the difficulty in maintaining a satisfactory detection performance over the large sensing areas. Furthermore, it is noteworthy from Fig. 6 that the increase in the number of cooperative BSs V brings remarkable increase of SDP and decrease of SOP, especially when V is small, owing to the increased intensity of echo signals and the decreased intensity of network clutter. However, further increasing V brings marginal performance improvement, which is restricted by the far distances between the target UAV and the newly involved cooperative BSs. Overall, appropriate choices of the BS sensing distance and number of cooperative BSs can significantly reduce the SOP whilst guaranteeing the SDP performance.

In Fig. 7, we study the impacts of BS density λ_{b} and the number of cooperative BSs V on SOP and RCP. The simulation results demonstrate that increasing λ_{b} brings a distinct rise in RCP. The denser the BSs, the lighter the communication load per BS, thus resulting in a performance improvement. On the other hand, with the increase of λ_{b}, the SOP in both standalone and cooperative sensing cases drops first and then rises. The reason is that, with small BS density and limited sensing distance per BS, a large proportion of UAVs are out of the sensing area of any of the BSs, implying the poor sensing coverage capability of the PMN. The increase in λ_{b} alleviates the sensing coverage issue, leading to the decline of SOP. However, too dense BS deployment takes a toll on SOP, due to the clutter caused by the large-scale BSs performing UAV surveillance simultaneously. In addition, the performance gain brought by the increase of V appears more significant when λ_{b} is large. This is because with dense BS deployment, BSs are close to each other and their sensing areas may overlap, which may lead to strong mutual interference. At this point, leveraging the V nearest BSs for cooperative sensing can significantly enhance the desired echo signals and reduce network clutter. Overall, under a dense BS deployment, increasing the number of cooperative BSs V can achieve a remarkable decline in SOP. However, for the sake of strong network clutter and high deployment cost, the BS density should not be too large.

C. Sensing Performance Optimization

To understand how the sensing outage performance of the mmWave PMN can be improved with the guarantee of both sensing detection and communication rate performance, Fig. 8 shows the relationships among the required SDP ϱ_{S}, required RCP ϱ_{C}, and minimal SOP $P_{\text{out}}^{\kappa^*}$ in standalone and cooperative sensing cases, by addressing the optimization problem in (33). A two-layer hierarchical search algorithm based on the alternating optimization is conducted, with the feasible ranges of parameters taking $\rho \in [0, 1]$, $\eta \in \{0, 0.1, \ldots, 1\}$, $\lambda_{\text{b}} \in [0.5, 10.5] \times 10^{-5}/\text{m}^2$, $R_{\text{S}} \in [20, 220]$ m, and $\Xi = 11$. Ten random initializations are implemented to approach global optimality. The obtained optimums under $\varrho_{\text{C}} = 0.8$ and $\varrho_{\text{S}} = 0.85$ are marked with red points in Fig. 8 as examples. It can be observed from the figure that, the minimal SOP under cooperative sensing at $V = 5$ drops by 92% as compared with that under standalone sensing at $V = 0$. It states that the cooperation among multiple BSs for sensing a UAV can significantly enhance the sensing coverage capability. Moreover, the optimal ρ, η, λ_{b}, and R_{S} indicate that with an increase in V for cooperative sensing, larger transmit power and more RF chains for sensing, larger sensing distance, and denser BS deployment can be configured to achieve a better sensing coverage performance, owing to the echo enhancement and clutter suppression by cooperation.

In addition, from the contour plots in Fig. 8, with fixed ϱ_{S}, a large ϱ_{C} leads to an increase in SOP. This is because the high requirement on RCP raises the demand of communication for power and RF chain resources, thus reducing the available resources for sensing and degrading the detection performance. On the other hand, with fixed ϱ_{C}, increasing ϱ_{S} brings remarkable rises in SOP. This indicates that, to guarantee the stringent requirement of each BS for successfully detecting its target UAVs, small sensing area and low BS density are demanded and thus the sensing coverage capability of the network is sacrificed. In addition, as shown in Figs. 8(b) and 8(c), only large ϱ_{C} and ϱ_{S} lead to the deterioration of minimal SOP, implying that cooperative sensing can jointly guarantee the UAV detection performance, sensing coverage, and communication performance unless with both stringent requirements on

RCP and SDP. It is elaborated in Fig. 8 that, by fine tuning the BS density, sensing distance, allocation of power and RF chain resources, and number of cooperative BSs, the PMN can strike a good balance between communication and sensing performance.

VIII. Conclusion

In this paper, we have analyzed the sensing and communication performance for mmWave UAV surveillance-oriented PMNs and investigated the interaction between the two functions. Specifically, we have developed a system-level theoretical framework based on stochastic geometry to investigate the rate coverage probability, successful detection probability, and sensing outage probability in both standalone and cooperative sensing cases. The analytical framework captures the mutual interference and resource contention between sensing and communication, and lays the foundation for network configuration and optimization. In addition, we have proposed a cooperative sensing strategy to achieve reliable UAV surveillance with the hybrid of monostatic sensing and bistatic sensing. Numerical and simulation results demonstrate that by appropriately setting key network parameters, the sensing performance can be optimized whilst guaranteeing communication requirements. Also, cooperative sensing can achieve great performance enhancement as compared with standalone sensing by reaping the spatial diversity gain from multiple collaborative BSs. For the future work, the theoretical framework can be extended to investigate the impacts of the imperfections in hardware, channel estimation, and beam alignment on both sensing and communication performance.

Appendix A. Proof of (3)

Given the typical BS located at the origin and the coordinate of an arbitrary GUE as $(x, y, -H_{\mathrm{B}})$, the virtual azimuth and elevation angles of the GUE relative to the typical BS are expressed as $\phi = \pi\cos\psi\sin\gamma = \pi x/\sqrt{x^2+y^2+H_{\mathrm{B}}^2} \in [-\pi, \pi]$ and $\theta = \pi\cos\gamma = -\pi H_{\mathrm{B}}/\sqrt{x^2+y^2+H_{\mathrm{B}}^2} \in [-\pi, \frac{-\pi H_{\mathrm{B}}}{\sqrt{D^2+H_{\mathrm{B}}^2}}]$, respectively, focusing on a circular region with radius D. The HPPP-distributed GUEs are uniformly distributed in the region, thus the joint PDF of the x and y coordinates of an arbitrary GUE is $f(x,y) = 1/\pi D^2$. Then, the joint PDF of the virtual azimuth and elevation angles of the GUE relative to the typical BS can be derived by $f_{\mathrm{C}}^{(\mathrm{ar})}(\phi,\theta) = f_{\mathrm{C}}^{(\mathrm{ar})}\big[x(\phi,\theta), y(\phi,\theta)\big]\left|\begin{matrix}\frac{\partial x}{\partial\phi} & \frac{\partial x}{\partial\theta}\\ \frac{\partial y}{\partial\phi} & \frac{\partial y}{\partial\theta}\end{matrix}\right|$. To sum up, the joint PDF of the virtual azimuth and elevation angles of an arbitrary GUE relative to the typical BS can be obtained as (3).

Appendix B. Proof of (20)

The RCP conditioned on K_0 GUEs in the coverage area of the typical BS is given by

$$P_{\mathrm{rate},K_0} = \mathbb{P}\Big[\tfrac{K}{K_0}B\log_2(1+\mathrm{SINR}_{K,k}) \geq \tau_{\mathrm{C}}\Big] = \mathbb{P}\bigg(\frac{TN_{\mathrm{t}}L_{\mathrm{C},\mathbf{x},k,e}\beta_{\mathrm{C},\mathbf{x},k,e}^2\frac{P_{\mathrm{t,C}}}{K}G_{\mathrm{t}}^2}{I_{\mathrm{intra,C}}+I_{\mathrm{intra,S}}+I_{\mathrm{inter}}+T\sigma_{\mathrm{C}}B} \geq \tau_{\mathrm{C},K_0}\bigg)$$

$$= \mathbb{E}_Q\mathbb{E}_{\delta_{k,i}}\bigg\{\int_0^\infty\Big\{\sum_{e\in\{\mathrm{L,N}\}}\mathbb{P}_e(v_0)\mathbb{P}\Big[\beta_{\mathrm{C},\mathbf{x},k,e}^2 \geq s_{e,0}\cdot \tau_{\mathrm{C},K_0}\big(\tfrac{I_{\mathrm{inter}}}{T}+\sigma_{\mathrm{C}}B\big)\Big]\mathbf{1}(s_{e,0}>0)\Big\}f_{\mathrm{G}}(v_0)\mathrm{d}v_0\bigg\}, \quad (34)$$

where $\tau_{\mathrm{C},K_0} = \exp[\tau_{\mathrm{C}}K_0\ln 2/(BK)] - 1$, $s_{e,0}^{-1} = \zeta N_{\mathrm{t}}\big\{\frac{P_{\mathrm{t,C}}}{K}G_{\mathrm{t}}^2 - \tau_{\mathrm{C},K_0}\frac{P_{\mathrm{t,C}}}{K}\sum_{i=1,i\neq k}^{K}[\delta_{k,i}G_{\mathrm{t}}^2 + (1-\delta_{k,i})g_{\mathrm{t}}^2] - \tau_{\mathrm{C},K_0}P_{\mathrm{t,S}}g_{\mathrm{t}}^2\mathbf{1}(Q\neq 0)\big\}(v_0^2+H_{\mathrm{B}}^2)^{-\frac{\alpha_e}{2}}, e\in\{\mathrm{L,N}\}$, and the indicator variable $\mathbf{1}(s_{e,0}>0)$ is added so that the inequality in (34) holds true. The inequality in (34) is further derived as

$$\begin{aligned}
&\mathbb{P}\Big[\beta_{\mathrm{C},\mathbf{x},k,e}^2 \geq s_{e,0}\tau_{\mathrm{C},K_0}\big(\tfrac{I_{\mathrm{inter}}}{T}+\sigma_{\mathrm{C}}B\big)\Big]\\
&\overset{(a)}{=} \mathbb{E}_{I_{\mathrm{inter}}}\bigg[\frac{\Gamma(m_e, s_e(\frac{I_{\mathrm{inter}}}{T}+\sigma_{\mathrm{C}}B))}{\Gamma(m_e)}\bigg]\\
&\overset{(b)}{=} \mathbb{E}_{I_{\mathrm{inter}}}\bigg\{\exp\Big[-s_e\big(\tfrac{I_{\mathrm{inter}}}{T}+\sigma_{\mathrm{C}}B\big)\Big]\sum_{c=0}^{m_e-1}\frac{\big[s_e(\frac{I_{\mathrm{inter}}}{T}+\sigma_{\mathrm{C}}B)\big]^c}{c!}\bigg\}\\
&\overset{(c)}{=} \sum_{c=0}^{m_e-1}\frac{s_e^c}{c!}\exp(-s_e\sigma_{\mathrm{C}}B)\sum_{l=0}^{c}\tbinom{c}{l}(-1)^{2c-l}(\sigma_{\mathrm{C}}B)^{(c-l)}\frac{\mathrm{d}^l\mathcal{L}_{I_{\mathrm{inter}}}(s_e)}{\mathrm{d}s_e^l},
\end{aligned} \quad (35)$$

where $s_e = m_e s_{e,0}\tau_{\mathrm{C},K_0}$; equation (a) comes from the complementary cumulative distribution function of the Gamma-distributed variable $\beta_{\mathrm{C},\mathbf{x},k,e}^2$; equation (b) follows from the expression of the upper incomplete Gamma function with m_e being an integer; equation (c) is yielded by $\exp\big[-s_e(I_{\mathrm{inter}}/T+\sigma_{\mathrm{C}}B)\big](I_{\mathrm{inter}}/T+\sigma_{\mathrm{C}}B)^c = (-1)^c\frac{\mathrm{d}^c}{\mathrm{d}s_e^c}\exp\big[-s_e(I_{\mathrm{inter}}/T+\sigma_{\mathrm{C}}B)\big]$ and the Leibniz integral formula. Furthermore, the Laplace transform in (35) is derived as

$$\begin{aligned}
&\mathcal{L}_{I_{\mathrm{inter}}}(s_e) = \mathbb{E}_{I_{\mathrm{inter}}}\Big[\exp(-s_e\tfrac{I_{\mathrm{inter}}}{T})\Big]\\
&= \prod_{K_0'=1}^{\infty}\prod_{e'\in\{\mathrm{L,N}\}}\mathbb{E}_{\Phi_{\mathrm{B}}^{(K_0')}}\bigg\{\prod_{\mathbf{x}'\in\Phi_{\mathrm{B}}^{(K_0')}\setminus\mathbf{x}}\exp\Big[-\frac{s_e}{T}\Big(\sum\nolimits_{i'=1}^{K'}\big\|\mathbf{h}_{\mathbf{x}',k}^{\mathrm{H}}\cdot \mathbf{w}_{\mathrm{C},\mathbf{x}',i'}\mathbf{s}_{\mathrm{C},\mathbf{x}',i'}\big\|^2 + \sum\nolimits_{j'=1}^{Q'}\big\|\mathbf{h}_{\mathbf{x}',k}^{\mathrm{H}}\mathbf{w}_{\mathrm{S},\mathbf{x}',j'}\mathbf{s}_{\mathrm{S},\mathbf{x}',j'}\big\|^2\Big)\Big]\bigg\}\\
&\overset{(a)}{=} \prod_{K'=1}^{\infty}\prod_{e'\in\{\mathrm{L,N}\}}\exp\bigg\{-2\pi\mathbb{P}(K_{\mathrm{G}}=K_0')\lambda_{\mathrm{b}}\frac{\int_0^\infty\mathbb{P}_{\mathrm{L}}(v)v\mathrm{d}v}{\int_0^\infty v\mathrm{d}v}\cdot \mathbb{E}_{Q'}\mathbb{E}_{\delta_{k,i'}}\bigg\{\int_{v_0}^{\infty}v\mathrm{d}v - \int_{v_0}^{\infty}\bigg[\frac{m_{e'}}{m_{e'}+\xi_1 s_e(v^2+H_{\mathrm{B}}^2)^{-\frac{\alpha_{e'}}{2}}}\bigg]^{m_{e'}}v\mathrm{d}v\bigg\}\bigg\},
\end{aligned} \quad (36)$$

where equation (a) comes from the probability generating functional (PGFL) of HPPP and the Gamma distribution of $\beta_{\mathrm{C},\mathbf{x}',k,e'}^2$. The integral in (36) can be further derived as

$$\begin{aligned}
&\int_{v_0}^{\infty}\bigg[\frac{m_{e'}}{m_{e'}+s_e\xi_1(v^2+H_{\mathrm{B}}^2)^{-\frac{\alpha_{e'}}{2}}}\bigg]^{m_{e'}}v\mathrm{d}v\\
&\overset{(a)}{=} \frac{1}{\alpha_{e'}}\int_{(v_0^2+H_{\mathrm{B}}^2)^{\frac{\alpha_{e'}}{2}}}^{\infty}\sum_{t=0}^{m_{e'}}\tbinom{m_{e'}}{t}(-1)^t\frac{\omega^{\frac{2}{\alpha_{e'}}-1}}{(1+m_{e'}s_e^{-1}\xi_1^{-1}\omega)^t}\mathrm{d}\omega\\
&\overset{(b)}{=} \int_{v_0}^{\infty}v\mathrm{d}v + \frac{1}{\alpha_{e'}}\sum_{t=1}^{m_{e'}}\tbinom{m_{e'}}{t}(-1)^t\frac{s_e^t\xi_1^t(v_0^2+H_{\mathrm{B}}^2)^{1-\frac{\alpha_{e'}t}{2}}}{(t-\frac{2}{\alpha_{e'}})m_{e'}^t}\cdot {}_2F_1\bigg(t, t-\tfrac{2}{\alpha_{e'}}; t-\tfrac{2}{\alpha_{e'}}+1; -\frac{\xi_1 s_e}{m_{e'}(v_0^2+H_{\mathrm{B}}^2)^{\frac{\alpha_{e'}}{2}}}\bigg),
\end{aligned} \quad (37)$$

where (a) comes from the substitution of $\omega=(v^2+H_{\mathrm{B}}^2)^{\frac{\alpha_{\mathrm{L}}'}{2}}$ and binomial expansion, (b) follows from the integral formula in [43][Eq. 3.194.2], with ${}_2F_1()$ being the Gaussian hypergeometric function. Combining (34)-(37), Theorem 1 is proved.

Appendix C. Proof of (26)

The SDP for the typical UAV under standalone sensing, conditioned on the number of UAVs in the sensing area of the typical BS Q_0, is given by

$$\begin{aligned}
&P_{\mathrm{det},Q_0}^{\mathrm{st}}=\frac{Q}{Q_0}\mathbb{P}(\mathrm{SCNR}_{Q,q}^{\mathrm{st}}\geq\tau_{\mathrm{S}})\\
&\overset{(a)}{=}\frac{Q}{Q_0}\mathbb{E}_K\mathbb{E}_{\delta_{q,j}}\mathbb{E}_{r_0}\left\{\exp\left[-s_{\mathrm{S}}\left(\tfrac{C_{\mathbf{x},q}^{\mathrm{st}}}{T}+\sigma_{\mathrm{S}}B\right)\right]\sum_{c=0}^{m_{\mathrm{L}}-1}\frac{\left[s_{\mathrm{S}}\left(\frac{C_{\mathbf{x},q}^{\mathrm{st}}}{T}+\sigma_{\mathrm{S}}B\right)\right]^c}{c!}\right\}\\
&=\frac{Q}{Q_0}\mathbb{E}_K\mathbb{E}_{\delta_{q,j}}\left\{\int_0^{R_{\mathrm{S}}}\sum_{c=0}^{m_{\mathrm{L}}-1}\frac{s_{\mathrm{S}}^c}{c!}\exp(-s_{\mathrm{S}}\sigma_{\mathrm{S}}B)\sum_{l=0}^{c}\binom{c}{l}(-1)^{2c-l}\cdot\right.\\
&\left.(\sigma_{\mathrm{S}}B)^{c-l}\frac{\mathrm{d}^l\mathcal{L}_{C_{\mathbf{x},q}^{(1)}}(s_{\mathrm{S}})\mathcal{L}_{C_{\mathbf{x},q}^{(2)}}(s_{\mathrm{S}})\mathcal{L}_{C_{\mathbf{x},q}^{(3)}}(s_{\mathrm{S}})\mathcal{L}_{C_{\mathbf{x},q}^{(4)}}(s_{\mathrm{S}})}{\mathrm{d}s_{\mathrm{S}}^l}f_{\mathrm{U}}(r_0)\mathrm{d}r_0\right\},\quad(38)
\end{aligned}$$

where equation (a) comes from the Gamma-distributed small-scale fading gain and the upper incomplete Gamma function. Specifically, $\mathcal{L}_{C_{\mathbf{x},q}^{(1)}}(s_{\mathrm{S}})$ in (38) can be further derived by

$$\begin{aligned}
&\mathcal{L}_{C_{\mathbf{x},q}^{(1)}}(s_{\mathrm{S}})=\mathbb{E}_{C_{\mathbf{x},q}^{(1)}}\left[\exp(-s_{\mathrm{S}}\tfrac{C_{\mathbf{x},q}^{(1)}}{T})\right]\\
&=\prod_{j=1,j\neq q}^{Q}\mathbb{E}_L\mathbb{E}_{\beta^2}\left\{\exp\left[-\delta_{q,j}\frac{s_{\mathrm{S}}}{T}\left\|\mathbf{a}_{\mathrm{r}}^{\mathrm{H}}(\phi_{\mathrm{S},\mathbf{x},q},\theta_{\mathrm{S},\mathbf{x},q})\mathbf{G}_{\mathbf{x},j,\mathbf{x}}\mathbf{X}\right\|^2\right]\right\}\\
&\overset{(a)}{=}\prod_{j=1,j\neq q}^{Q}\int_0^{R_{\mathrm{S,max}}}\left[\frac{m_{\mathrm{L}}}{m_{\mathrm{L}}+s_{\mathrm{S}}\xi_2({\nu_0}^2+\Delta H^2)^{-\alpha_{\mathrm{L}}}}\right]^{m_{\mathrm{L}}}f_{\mathrm{U}}(\nu_0)\mathrm{d}\nu_0\\
&=\prod_{j=1,j\neq q}^{Q}\frac{1}{\alpha_{\mathrm{L}}R_{\mathrm{S}}^2}\sum_{t=0}^{m}\binom{m}{t}(-1)^t\left[\frac{\Delta H^{2-2\alpha_{\mathrm{L}}t}\xi_2^t s_{\mathrm{S}}^t}{m_{\mathrm{L}}^t(t-\frac{1}{\alpha_{\mathrm{L}}})}{}_2F_1\left(t,t-\frac{1}{\alpha_{\mathrm{L}}};\right.\right.\\
&\left.t-\frac{1}{\alpha_{\mathrm{L}}}+1;-\frac{\xi_2 s_{\mathrm{S}}}{m_{\mathrm{L}}\Delta H^{2\alpha_{\mathrm{L}}}}\right)-\frac{(R_{\mathrm{S,max}}^2+\Delta H^2)^{1-\alpha_{\mathrm{L}}t}\xi_2^t s_{\mathrm{S}}^t}{m_{\mathrm{L}}^t(t-\frac{1}{\alpha_{\mathrm{L}}})}\cdot\\
&\left.{}_2F_1\left(t,t-\frac{1}{\alpha_{\mathrm{L}}};t-\frac{1}{\alpha_{\mathrm{L}}}+1;-\frac{\xi_2 s_{\mathrm{S}}}{m_{\mathrm{L}}(R_{\mathrm{S,max}}^2+\Delta H^2)^{\alpha_{\mathrm{L}}}}\right)\right],\quad(39)
\end{aligned}$$

where coefficient $\xi_2=\frac{\bar{\sigma}}{4\pi}\zeta\delta_{q,j}G_{\mathrm{r}}^2N_{\mathrm{r}}N_{\mathrm{t}}\left\{P_{\mathrm{t,C}}g_{\mathrm{t}}^2\mathbf{1}(K\neq0)+\frac{P_{\mathrm{t,S}}}{Q}G_{\mathrm{t}}^2+\sum_{j=1,j\neq q}^{Q}\frac{P_{\mathrm{t,S}}}{Q}[\delta_{q,j}G_{\mathrm{t}}^2+(1-\delta_{q,j})g_{\mathrm{t}}^2]\right\}$, and equation (a) results from the Gamma-distributed variable $\beta_{\mathrm{S},\mathbf{x},j,\mathbf{x}}^2$. In addition, $\mathcal{L}_{C_{\mathbf{x},q}^{(2)}}(s_{\mathrm{S}})$ in (38) can be obtained by

$$\begin{aligned}
&\mathcal{L}_{C_{\mathbf{x},q}^{(2)}}(s_{\mathrm{S}})=\mathbb{E}_{\Phi_{\mathrm{B}}^{(q)}}\left\{\prod_{\mathbf{x}'\in\Phi_{\mathrm{B}}^{(q)}\setminus\mathbf{x}}\exp\left[-\frac{s_{\mathrm{S}}}{T}\left\|\mathbf{a}_{\mathrm{r}}^{\mathrm{H}}(\phi_{\mathrm{S},\mathbf{x},q},\theta_{\mathrm{S},\mathbf{x},q})\mathbf{G}_{\mathbf{x}',q,\mathbf{x}}\mathbf{X}'\right\|^2\right]\right\}\\
&\overset{(a)}{=}\prod_{Q_0'=1}^{\infty}\exp\left\{-2\pi\mathbb{P}(Q_{\mathrm{U}}=Q_0')\lambda_{\mathrm{b}}\mathbb{E}_{K'}\mathbb{E}_{\delta_{q,j'}}\left\{\int_0^{\infty}\left\{1-\right.\right.\right.\\
&\left.\left.\left.\left[\frac{m_{\mathrm{L}}}{m_{\mathrm{L}}+s_{\mathrm{S}}\xi_3\left[(\nu_1^2+\Delta H^2)(r_0^2+\Delta H^2)\right]^{-\frac{\alpha_{\mathrm{L}}}{2}}}\right]^{m_{\mathrm{L}}}\right\}\nu_1\mathrm{d}\nu_1\right\}\right\}\\
&=\prod_{Q_0'=1}^{\infty}\exp\left\{\frac{2\pi}{\alpha_{\mathrm{L}}}\mathbb{P}(Q_{\mathrm{U}}=Q_0')\lambda_{\mathrm{b}}\mathbb{E}_{K'}\mathbb{E}_{\delta_{q,j'}}\left[\sum_{t=1}^{m_{\mathrm{L}}}\binom{m_{\mathrm{L}}}{t}\frac{(-1)^t\xi_3^t s_{\mathrm{S}}^t}{(t-\frac{2}{\alpha_{\mathrm{L}}})m_{\mathrm{L}}^t}\cdot\right.\right.\\
&\left.\left.\frac{(\nu_{\min}^2+\Delta H^2)^{\frac{2-\alpha_{\mathrm{L}}t}{2}}}{(r_0^2+\Delta H^2)^{\frac{\alpha_{\mathrm{L}}t}{2}}}{}_2F_1\left(t,t-\frac{2}{\alpha_{\mathrm{L}}};t-\frac{2}{\alpha_{\mathrm{L}}}+1;-\frac{\xi_3 s_{\mathrm{S}}(r_0^2+\Delta H^2)^{-\frac{\alpha_{\mathrm{L}}}{2}}}{m_{\mathrm{L}}(\nu_{\min}^2+\Delta H^2)^{\frac{\alpha_{\mathrm{L}}}{2}}}\right)\right]\right\},\quad(40)
\end{aligned}$$

where coefficient $\xi_3=\frac{\bar{\sigma}}{4\pi}\zeta G_{\mathrm{r}}^2N_{\mathrm{r}}N_{\mathrm{t}}\left\{P_{\mathrm{t,C}}g_{\mathrm{t}}^2\mathbf{1}(K'\neq0)+\frac{P_{\mathrm{t,S}}}{Q'}G_{\mathrm{t}}^2+\sum_{j'=1}^{Q'-1}\frac{P_{\mathrm{t,S}}}{Q'}[\delta_{q,j'}G_{\mathrm{t}}^2+(1-\delta_{q,j'})g_{\mathrm{t}}^2]\right\}$; $\nu_{\min}$ is the minimum horizontal distance between interfering BSs and the typical UAV, equal to 0 implying the interfering BSs can be infinitely close to the typical UAV; and equation (a) is derived from the property of Gamma distribution and the PGFL of HPPP. $\mathcal{L}_{C_{\mathbf{x},q}^{(3)}}(s_{\mathrm{S}})$ in (38) can be similarly obtained by

$$\begin{aligned}
&\mathcal{L}_{C_{\mathbf{x},q}^{(3)}}(s_{\mathrm{S}})=\exp\left[\frac{\pi\lambda_{\mathrm{u}}p_{\mathrm{main,S,2}}}{\alpha_{\mathrm{L}}}\sum_{t=1}^{m_{\mathrm{L}}}\binom{m_{\mathrm{L}}}{t}(-1)^t\frac{\Delta H^{2-2\alpha_{\mathrm{L}}t}\xi_4^t s_{\mathrm{S}}^t}{(t-\frac{1}{\alpha_{\mathrm{L}}})m_{\mathrm{L}}^t}\cdot\right.\\
&\left.{}_2F_1\left(t,t-\frac{1}{\alpha_{\mathrm{L}}};t-\frac{1}{\alpha_{\mathrm{L}}}+1;-\frac{\xi_4 s_{\mathrm{S}}}{m_{\mathrm{L}}\Delta H^{2\alpha_{\mathrm{L}}}}\right)\right],\quad(41)
\end{aligned}$$

with coefficient $\xi_4=\frac{\bar{\sigma}}{4\pi}\zeta G_{\mathrm{r}}^2N_{\mathrm{r}}N_{\mathrm{t}}\left\{P_{\mathrm{t,C}}g_{\mathrm{t}}^2\mathbf{1}(K\neq0)+\frac{P_{\mathrm{t,S}}}{Q}G_{\mathrm{t}}^2+\sum_{j=1,j\neq q}^{Q}\frac{P_{\mathrm{t,S}}}{Q}[\delta_{q,j}G_{\mathrm{t}}^2+(1-\delta_{q,j})g_{\mathrm{t}}^2]\right\}$. The Laplace transform of $C_{\mathbf{x},q}^{(4)}$ in (38) can be obtained by

$$\begin{aligned}
&\mathcal{L}_{C_{\mathbf{x},q}^{(4)}}(s_{\mathrm{S}})=\exp\left\{\frac{2\pi\lambda_{\mathrm{u}}p_{\mathrm{main,S,2}}}{\alpha_{\mathrm{L}}}\mathbb{E}_{K'}\mathbb{E}_{Q'}\mathbb{E}_{\delta_{u,j'}}\int_0^{\infty}\left\{\sum_{t=1}^{m_{\mathrm{L}}}\right.\right.\\
&\binom{m_{\mathrm{L}}}{t}\frac{(-1)^t\Delta H^{2-\alpha_{\mathrm{L}}t}\xi_5^t s_{\mathrm{S}}^t}{(t-\frac{2}{\alpha_{\mathrm{L}}})(\nu_3^2+\Delta H^2)^{\frac{\alpha_{\mathrm{L}}t}{2}}m_{\mathrm{L}}^t}{}_2F_1\left(t,t-\frac{2}{\alpha_{\mathrm{L}}};\ t-\frac{2}{\alpha_{\mathrm{L}}}+1;\right.\\
&\left.\left.\left.-\frac{\xi_5 s_{\mathrm{S}}({\nu_3}^2+\Delta H^2)^{-\frac{\alpha_{\mathrm{L}}}{2}}}{m_{\mathrm{L}}\Delta H^{\alpha_{\mathrm{L}}}}\right)\right\}f_{Q',u}(\nu_3)\mathrm{d}\nu_3\right\},\quad(42)
\end{aligned}$$

where coefficient $\xi_5=\frac{\bar{\sigma}}{4\pi}\zeta G_{\mathrm{r}}^2N_{\mathrm{r}}N_{\mathrm{t}}\left\{P_{\mathrm{t,C}}g_{\mathrm{t}}^2\mathbf{1}(K'\neq0)+\frac{P_{\mathrm{t,S}}}{Q'}G_{\mathrm{t}}^2+\sum_{j'=1}^{Q'-1}\frac{P_{\mathrm{t,S}}}{Q'}[\delta_{u,j'}G_{\mathrm{t}}^2+(1-\delta_{u,j'})g_{\mathrm{t}}^2]\right\}$; $\delta_{u,j'}$ equals 1 with probability $p_{\mathrm{main,S,2}}$ and 0 otherwise; and $f_{Q_0',u}(\nu_3)=2\pi\lambda_{\mathrm{b}}[1-(1-p_{\mathrm{main,S,2}})^{Q'}]\mathbb{P}(Q_{\mathrm{U}}=Q_0')\nu_3\exp\left\{-\lambda_{\mathrm{b}}[1-(1-p_{\mathrm{main,S,2}})^{Q'}]\mathbb{P}(Q_{\mathrm{U}}=Q_0')\pi\nu_3^2\right\}$ is the PDF of the horizontal distance between the UAV u and its nearest interfering BS with main lobe interference and of Q' target UAVs, which can be obtained based on the empty space probability of HPPP.

Appendix D. Proof of (30)

For cooperative sensing with V cooperative BSs, the SDP of the typical BS for the typical UAV, given the number of UAVs in the sensing area of the typical BS Q_0, is given by

$$\begin{aligned}
&P_{\mathrm{det},Q_0}^{\mathrm{co}}=\tfrac{Q}{Q_0}\mathbb{P}(\mathrm{SCNR}_{Q,q}^{\mathrm{co}}\geq\tau_{\mathrm{S}})\\
&\overset{(a)}{\approx}\frac{Q}{Q_0}\mathbb{E}_{Q_{V,1},\ldots,Q_{V,V}}\mathbb{E}_{r_0,r_1,\ldots,r_V}\left\{\frac{\Gamma\left[\tilde{\epsilon},\tilde{\mu}\tau_{\mathrm{S}}(\frac{C_{\mathbf{x},q}^{\mathrm{co}}}{T}+\sigma_{\mathrm{S}}B)\right]}{\Gamma(\tilde{\epsilon})}\right\}\\
&\overset{(b)}{<}\frac{Q}{Q_0}\left\{1-\mathbb{E}_{Q_{V,1},\ldots,Q_{V,V}}\mathbb{E}_{r_0,r_1,\ldots,r_V}\left\{1-\right.\right.\\
&\left.\left.\exp\left\{-\left[\Gamma(1+\tilde{\epsilon})\right]^{-\frac{1}{\tilde{\epsilon}}}\tilde{\mu}\tau_{\mathrm{S}}(\tfrac{C_{\mathbf{x},q}^{\mathrm{co}}}{T}+\sigma_{\mathrm{S}}B)\right\}\right\}^{\tilde{\epsilon}}\right\}\\
&\overset{(c)}{=}\frac{Q}{Q_0}\left\{1-\sum_{z=0}^{\infty}\frac{(-1)^z}{z!}\mathbb{E}_{Q_{V,1},\ldots,Q_{V,V}}\left\{\int_0^{R_{\mathrm{S}}}\int_0^{\infty}\int_{r_1}^{\infty}\cdots\int_{r_{V-1}}^{\infty}\prod_{t=0}^{z-1}(\tilde{\epsilon}-t)\cdot\right.\right.\\
&\left.\left.\exp\left\{-z\left[\Gamma(1+\tilde{\epsilon})\right]^{-\frac{1}{\tilde{\epsilon}}}\tilde{\mu}\tau_{\mathrm{S}}\sigma_{\mathrm{S}}B\right\}\mathcal{L}_{C_{\mathbf{x},q}^{\mathrm{co}}}\left(z\left[\Gamma(1+\tilde{\epsilon})\right]^{-\frac{1}{\tilde{\epsilon}}}\tilde{\mu}\tau_{\mathrm{S}}\right)\cdot\right.\right.
\end{aligned}$$

$$f_{\mathrm{U}}(r_0) f_V^{\mathrm{co}}(r_1, r_2, \cdots, r_V) \mathrm{d}r_V \mathrm{d}r_{V-1} \cdots \mathrm{d}r_0 \Bigg\} \Bigg\}, \quad (43)$$

where step (a) comes from the Gamma approximation given in Lemma 1, with shape and rate parameters $\tilde{\epsilon}$ and $\tilde{\mu}$ given in (31); (b) comes from the Alzer's inequality for the incomplete Gamma function [44]; step (c) holds due to the generalized binomial theorem; and $f_V^{\mathrm{co}}(r_1, r_2, \cdots, r_V)$ is given in (15).

REFERENCES

[1] F. Liu *et al.*, "Integrated sensing and communications: Toward dual-functional wireless networks for 6G and beyond," *IEEE J. Sel. Areas Commun.*, vol. 40, no. 6, pp. 1728–1767, Jun. 2022.

[2] J. A. Zhang *et al.*, "Enabling joint communication and radar sensing in mobile networks-A survey," *IEEE Commun. Surv. Tutor.*, vol. 24, no. 1, pp. 306–345, 1st Quart., 2022.

[3] F. Liu *et al.*, "Joint radar and communication design: Applications, state-of-the-art, and the road ahead," *IEEE Trans. Commun.*, vol. 68, no. 6, pp. 3834–3862, Jun. 2020.

[4] N. Cheng *et al.*, "Air-ground integrated mobile edge networks: Architecture, challenges, and opportunities," *IEEE Commun. Mag.*, vol. 56, no. 8, pp. 26–32, Aug. 2018.

[5] F. Dong, F. Liu, Y. Cui, W. Wang, K. Han, and Z. Wang, "Sensing as a service in 6G perceptive networks: A unified framework for ISAC resource allocation," *IEEE Trans. Wireless Commun.*, vol. 22, no. 5, pp. 3522–3536, May 2023.

[6] H. Wu, X. Tao, N. Zhang, and X. Shen, "Cooperative UAV cluster-assisted terrestrial cellular networks for ubiquitous coverage," *IEEE J. Sel. Areas Commun.*, vol. 36, no. 9, pp. 2045–2058, Sep. 2018.

[7] Q. Wu *et al.*, "A comprehensive overview on 5G-and-beyond networks with UAVs: From communications to sensing and intelligence," *IEEE J. Sel. Areas Commun.*, vol. 39, no. 10, pp. 2912–2945, Oct. 2021.

[8] X. Shi, C. Yang, W. Xie, C. Liang, Z. Shi, and J. Chen, "Anti-drone system with multiple surveillance technologies: Architecture, implementation, and challenges," *IEEE Commun. Mag.*, vol. 56, no. 4, pp. 68–74, Apr. 2018.

[9] M. L. Rahman, J. A. Zhang, X. Huang, Y. J. Guo, and R. W. Heath, "Framework for a perceptive mobile network using joint communication and radar sensing," *IEEE Trans. Aerosp. Electron. Syst.*, vol. 56, no. 3, pp. 1926–1941, Jun. 2020.

[10] Y. Zhang, H. Shan, H. Chen, D. Mi, and Z. Shi, "Perceptive mobile networks for unmanned aerial vehicle surveillance: From the perspective of cooperative sensing," *IEEE Veh. Technol. Mag.*, pp. 2–11, Mar. 2024.

[11] L. Xie, S. Song, Y. C. Eldar, and K. B. Letaief, "Collaborative sensing in perceptive mobile networks: Opportunities and challenges," *IEEE Wireless Commun.*, vol. 30, no. 1, pp. 16–23, Feb. 2023.

[12] B. Li, A. P. Petropulu, and W. Trappe, "Optimum co-design for spectrum sharing between matrix completion based MIMO radars and a MIMO communication system," *IEEE Trans. Signal Process.*, vol. 64, no. 17, pp. 4562–4575, Sep. 2016.

[13] F. Liu, Y.-F. Liu, A. Li, C. Masouros, and Y. C. Eldar, "Cramér-Rao bound optimization for joint radar-communication beamforming," *IEEE Trans. Signal Process.*, vol. 70, pp. 240–253, Jan. 2022.

[14] L. Xie, P. Wang, S. Song, and K. B. Letaief, "Perceptive mobile network with distributed target monitoring terminals: Leaking communication energy for sensing," *IEEE Trans. Wireless Commun.*, vol. 21, no. 12, pp. 10 193–10 207, Dec. 2022.

[15] C. Skouroumounis, C. Psomas, and I. Krikidis, "Cooperative detection for mmWave radar-communication systems," in *Proc. IEEE Int. Conf. Commun. Workshops (ICC Workshops)*, Jun. 2020, pp. 1–6.

[16] J. Ge, H. Wang, G. Liu, and W. Lv, "The design and implementation of multi-radar signal-level cooperative detection system," in *Proc. CIE Int. Conf. Radar (Radar)*, Dec. 2021, pp. 2636–2640.

[17] M. Alzenad and H. Yanikomeroglu, "Coverage and rate analysis for vertical heterogeneous networks (VHetNets)," *IEEE Trans. Wireless Commun.*, vol. 18, no. 12, pp. 5643–5657, Dec. 2019.

[18] Q. Shi, L. Liu, S. Zhang, and S. Cui, "Device-free sensing in OFDM cellular network," *IEEE J. Sel. Areas Commun.*, vol. 40, no. 6, pp. 1838–1853, Jun. 2022.

[19] X. Li, J. Fang, H. Duan, Z. Chen, and H. Li, "Fast beam alignment for millimeter wave communications: A sparse encoding and phaseless decoding approach," *IEEE Trans. Signal Process.*, vol. 67, no. 17, pp. 4402–4417, Sep. 2019.

[20] M. N. Kulkarni *et al.*, "A comparison of MIMO techniques in downlink millimeter wave cellular networks with hybrid beamforming," *IEEE Trans. Commun.*, vol. 64, no. 5, pp. 1952–1967, May 2016.

[21] Y. Song *et al.*, "Joint spatial division and multiplexing in massive MIMO: A neighbor-based approach," *IEEE Trans. Wireless Commun.*, vol. 19, no. 11, pp. 7392–7406, Nov. 2020.

[22] J. Li, A. Huang, H. Shan, H. H. Yang, and T. Q. S. Quek, "Analysis of packet throughput in small cell networks under clustered dynamic TDD," *IEEE Trans. Wireless Commun.*, vol. 17, no. 9, pp. 5729–5742, Sep. 2018.

[23] F. Járai-Szabó and Z. Néda, "On the size-distribution of poisson voronoi cells," *Physica A., Statist. Mech. Appl.*, vol. 385, no. 2, pp. 518–526, Jul. 2004.

[24] M. Chung, L. Liu, and O. Edfors, "Phase-noise compensation for OFDM systems exploiting coherence bandwidth: Modeling, algorithms, and analysis," *IEEE Trans. Wireless Commun.*, vol. 21, no. 5, pp. 3040–3056, May 2022.

[25] Y. Xiong, F. Liu, Y. Cui, W. Yuan, T. X. Han, and G. Caire, "On the fundamental tradeoff of integrated sensing and communications under gaussian channels," *IEEE Trans. Inf. Theory*, vol. 69, no. 9, pp. 5723–5751, Jun. 2023.

[26] S. D. Liyanaarachchi, T. Riihonen, C. B. Barneto, and M. Valkama, "Optimized waveforms for 5G–6G communication with sensing: Theory, simulations and experiments," *IEEE Trans. Wireless Commun.*, vol. 20, no. 12, pp. 8301–8315, Jun. 2021.

[27] U. Madhow, *Fundamentals of Digital Communication*. Cambridge University Press, 2008.

[28] S. Zhang *et al.*, "Energy-efficient massive MIMO with decentralized precoder design," *IEEE Trans. Veh. Technol.*, vol. 69, no. 12, pp. 15 370–15 384, Dec. 2020.

[29] M. Giordani, M. Polese, A. Roy, D. Castor, and M. Zorzi, "Standalone and non-standalone beam management for 3GPP NR at mmwaves," *IEEE Commun. Mag.*, vol. 57, no. 4, pp. 123–129, Apr. 2019.

[30] A. Al-Hourani *et al.*, "Optimal LAP altitude for maximum coverage," *IEEE Wireless Commun. Lett.*, vol. 3, no. 6, pp. 569–572, Dec. 2014.

[31] Z. Hong, K. Liu, R. Heath, and A. Sayeed, "Spatial multiplexing in correlated fading via the virtual channel representation," *IEEE J. Sel. Areas Commun.*, vol. 21, no. 5, pp. 856–866, Jun. 2003.

[32] T. Bai and R. W. Heath, "Coverage and rate analysis for millimeter-wave cellular networks," *IEEE Trans. Wireless Commun.*, vol. 14, no. 2, pp. 1100–1114, Feb. 2015.

[33] D. Kim, J. Lee, and T. Q. S. Quek, "Multi-layer unmanned aerial vehicle networks: Modeling and performance analysis," *IEEE Trans. Wireless Commun.*, vol. 19, no. 1, pp. 325–339, Jan. 2020.

[34] H. Du *et al.*, "Semantic communications for wireless sensing: RIS-aided encoding and self-supervised decoding," *IEEE J. Sel. Areas Commun.*, vol. 41, no. 8, pp. 2547–2562, Aug. 2023.

[35] Y. Zhong, T. Q. S. Quek, and X. Ge, "Heterogeneous cellular networks with spatio-temporal traffic: Delay analysis and scheduling," *IEEE J. Sel. Areas Commun.*, vol. 35, no. 6, pp. 1373–1386, Jun. 2017.

[36] R. S. Esfandiari, *Numerical Methods For Engineers and Scientists Using MATLAB®*. CRC Press, 2017.

[37] W. H. Press, *Numerical Recipes 3rd Edition: The Art of Scientific Computing*. Cambridge University Press, 2007.

[38] C.-S. Choi, J. O. Woo, and J. G. Andrews, "An analytical framework for modeling a spatially repulsive cellular network," *IEEE Trans. Commun.*, vol. 66, no. 2, pp. 862–874, Feb. 2018.

[39] A. Munari, L. Simić, and M. Petrova, "Stochastic geometry interference analysis of radar network performance," *IEEE Commun. Lett.*, vol. 22, no. 11, pp. 2362–2365, Nov. 2018.

[40] R. W. Heath Jr, T. Wu, Y. H. Kwon, and A. C. K. Soong, "Multiuser MIMO in distributed antenna systems with out-of-cell interference," *IEEE Trans. Signal Process.*, vol. 59, no. 10, pp. 4885–4899, Oct. 2011.

[41] D. Bertsekas, *Nonlinear Programming*. Athena Scientific, 2016.

[42] P. Burt and E. Adelson, "The laplacian pyramid as a compact image code," *IEEE Trans. Commun.*, vol. 31, no. 4, pp. 532–540, Apr. 1983.

[43] I. S. Gradshteĭn, I. M. Ryzhik, and A. Jeffrey, *Table of Integrals, Series, and Products*. Academic press, 2007.

[44] H. Alzer, "On some inequalities for the incomplete gamma function," *Math. Comput.*, vol. 66, no. 218, pp. 771–778, Apr. 1997.

Yue Zhang received the B.Eng. degree in communication engineering from Nanchang University, Nanchang, China, in 2020. She is currently pursuing the Ph.D. degree with the Institute of Information and Communication Network Engineering, Zhejiang University, Hangzhou, China. Her research interests include the design and optimization of the UAV-assisted cellular networks and integrated sensing and communication networks.

Hangguan Shan (Senior Member, IEEE) received the B.Sc. degree in electrical engineering from Zhejiang University, Hangzhou, China, in 2004, and the Ph.D. degree in electrical engineering from Fudan University, Shanghai, China, in 2009. From 2009 to 2010, he was a Post-Doctoral Research Fellow with the University of Waterloo, Waterloo, ON, Canada. Since 2011, he has been with the College of Information Science and Electronic Engineering, Zhejiang University, where he is currently an Associate Professor. He is also with Zhejiang Provincial Key Laboratory of Information Processing and Communication Networks, Zhejiang University. His current research interests include machine learning-enabled resource allocation and quality-of-service provisioning in wireless networks. He has co-received the Best Industry Paper Award from the IEEE WCNC'11 and the Best Paper Award from the IEEE WCSP'23. He has served as a technical program committee member for various international conferences. He is an Associate Editor of the IET Communications. He was an Editor of IEEE TRANSACTIONS ON GREEN COMMUNICATIONS AND NETWORKING.

Hongbin Chen received the B.Eng. degree in and information engineering from Nanjing University of Posts and Telecommunications,Nanjing, China, in 2004 and the Ph.D. degree in circuits and systems from South China University of Technology, Guangzhou, China, in 2009. From October 2006 to May 2008, he was a Research Assistant with the Department of Electronic and Information Engineering, Hong Kong Polytechnic University, Hong Kong. From March to April 2014, he was a Research Associate with the same department. From May 2015 to May 2016, he was a Visiting Scholar with the Department of Electrical and Computer Engineering, National University of Singapore, Singapore. He is currently a Professor with the School of Information and Communication, Guilin University of Electronic Technology, Guilin, China. His research interests include energy-efficient wireless communications.

Lin Cai (Fellow, IEEE) has been with the Department of Electrical & Computer Engineering at the University of Victoria since 2005, and she is currently a Professor. She is an NSERC E.W.R. Steacie Memorial Fellow, an Engineering Institute of Canada Fellow, a Canadian Academy of Engineering Fellow, and an IEEE Fellow. In 2020, she was elected as a Member of the Royal Society of Canada's College of New Scholars, Artists and Scientists, and a 2020 "Star in Computer Networking and Communications" by N2Women. Her research interests span several areas in communications and networking, with a focus on network protocol and architecture design supporting emerging multimedia traffic and the Internet of Things. She has been elected to serve the board of the IEEE Vehicular Technology Society, 2019 - 2024, and as its VP in Mobile Radio. She has been a Board Member of IEEE Women in Engineering (2022-24) and IEEE Communications Society (2024-2026). She has served as an Associate Editor-in-Chief for IEEE Transactions on Vehicular Technology, and as a Distinguished Lecturer of the IEEE VTS Society and the IEEE Communications Society.

Zhiguo Shi (Senior Member, IEEE) received the B.S. and Ph.D. degrees in Electronic Engineering from Zhejiang University, Hangzhou, China, in 2001 and 2006, respectively. Since 2006, he has been a Faculty Member with the College of Information Science and Electronic Engineering, Zhejiang University, where he is currently a Full Professor. From 2011 to 2013, he visited the Broadband Communications Research Group, University of Waterloo, Waterloo, ON, Canada. His research interests include array signal processing, localization, and internet-of-things.

Prof. Shi was the recipient of the 2019 IET Communications Premium Award, and coauthored a paper that received the 2021 IEEE Signal Processing Society Young Author Best Paper Award. He was also the recipient of the Best Paper Award from ISAP 2020, IEEE GLOBECOM 2019, IEEE WCNC 2017, IEEE/CIC ICCC 2013, and IEEE WCNC 2013. He was the General Co-Chair of IEEE SAM 2020 and served as an Editor for the IEEE Network. He is currently serving as an Associate Editor for the IEEE Signal Processing Letters, IEEE Transactions on Vehicular Technology, and Journal of the Franklin Institute. He is an elected member of the Sensor Array and Multichannel (SAM) Technical Committee of the IEEE Signal Processing Society.

Tony Q. S. Quek (Fellow, IEEE) received the B.E. and M.E. degrees in electrical and electronics engineering from the Tokyo Institute of Technology in 1998 and 2000, respectively, and the Ph.D. degree in electrical engineering and computer science from the Massachusetts Institute of Technology in 2008. Currently, he is the Cheng Tsang Man Chair Professor with Singapore University of Technology and Design (SUTD) and ST Engineering Distinguished Professor. He also serves as the Director of the Future Communications R&D Programme, the Head of ISTD Pillar, and the AI on RAN Working Group Chair in AI-RAN Alliance. His current research topics include wireless communications and networking, network intelligence, non-terrestrial networks, open radio access network, and 6G.

Dr. Quek has been actively involved in organizing and chairing sessions, and has served as a member of the Technical Program Committee as well as symposium chairs in a number of international conferences. He is currently serving as an Area Editor for the IEEE TRANSACTIONS ON WIRELESS COMMUNICATIONS.

Dr. Quek was honored with the 2008 Philip Yeo Prize for Outstanding Achievement in Research, the 2012 IEEE William R. Bennett Prize, the 2015 SUTD Outstanding Education Awards – Excellence in Research, the 2016 IEEE Signal Processing Society Young Author Best Paper Award, the 2017 CTTC Early Achievement Award, the 2017 IEEE ComSoc AP Outstanding Paper Award, the 2020 IEEE Communications Society Young Author Best Paper Award, the 2020 IEEE Stephen O. Rice Prize, the 2020 Nokia Visiting Professor, the 2022 IEEE Signal Processing Society Best Paper Award, and the 2024 IIT Bombay International Award For Excellence in Research in Engineering and Technology. He is an IEEE Fellow, a WWRF Fellow, and a Fellow of the Academy of Engineering Singapore.

Li Sheng received the Ph.D. degree in Electronic Engineering from Zhejiang University, Hangzhou, China, in 2000, and he is currently the Chief Consulting Engineer of Huaxin Consulting Research Institute Co., Ltd., Hangzhou, China. He has been engaged in research and consulting work in the areas of telecommunications industry network construction planning and digitalization for an extended period. The projects he has overseen received numerous national and industry awards, including the First-Class Prize for Excellent Telecommunication Consulting Achievements, and the First-Class Science and Technology Award from the Zhejiang Provincial Telecommunications Association.